Representativeness of global climate and vegetation by carbon-monitoring networks; implications for estimates of gross and net primary productivity at biome and global levels

Paul B. Alton, Geography Dept., Swansea University, SA2 8PP, UK.
p.alton@swansea.ac.uk +44(0)1792 295069

March 11, 2020

1 Abstract

One of the major uncertainties in estimating global Net Primary Productivity (NPP) and Gross Primary Productivity (GPP) is the ability of carbon-monitoring sites to represent the climate and canopy-density of global vegetation ("representativeness"). These sites are used for empirical upscaling and calibration of global land-surface models. The current study determines the representativeness of two important carbon-monitoring networks – FLUXNET2015 and the Ecosystem Model-Data Intercomparison (EMDI) – by calculating the euclidian distance in climate-canopy space between each global 0.5° cell and all carbon-monitoring sites of the same biome or Plant Functional Type (PFT). Reliance on the single (most similar) site has been adopted in the past. A straightforward weighted upscaling, using inverse euclidian distance, identifies which PFTs contribute most to global primary productivity in the context of how well they are represented in carbon-monitoring networks. Some vegetation types, which are numerically well-represented within the network, are sampled at the 'wrong' latitude and in more temperate climes than their global distribution. This includes non-mediterranean needleleaf forest which is one of the main vegetation types contributing to global GPP and NPP. (Semi-)arid regions (mean annual precipitation <400 mm yr^{-1}) are undersampled as well as the sparse vegetation that tends to characterise them. These regions include the tundra and the northern half of the boreal forest where growth is disproportionately affected by climate change. We find a large spread in NPP and GPP recorded at sites of the same PFT (standard deviation is 56% mean). Consequently, our bootstrap error analysis indicates that a minimum of 50 climate-representative sites per PFT is required to quantify adequately (2% precision) the primary productivity of each global vegetation type. Selecting unchartered climate-canopy space for new sites appears to be more important than a simple increase in site numbers.

Keywords

Gross Primary Productivity (GPP); Net Primary Productivity (NPP); representativeness; MODIS; land-surface modelling; Plant Functional Types;

Highlights

- global productivity dominated by tropical/needleleaf forest & C3 grass/crops
- well sampled PFTs (e.g. needleleaf forest) sampled at wrong latitude & climate
- (semi-)arid (MAP$<$400 mm yr^{-1}) & sparse (LAI$\leq$2 m^{2}m^{-2}) vegetation undersampled
- each PFT requires $>$50 climate-representative sites to determine its productivity

2 Introduction

Estimates of NPP and GPP (see Tab. 1 for acronyms used frequently in the text) at PFT and global levels are still uncertain, despite their importance to the terrestrial carbon-cycle and rising atmospheric CO_2 concentration (Keenan et al 2016). For example, model estimates of global NPP vary by ±20% (55±11 Gt yr^{-1}; Cramer et al 1999; Ito 2011), whilst anthropogenic carbon release is less than this dispersion (9 Gt yr^{-1}; Le Quéré et al 2015). Therefore, our precision in quantifying the fluxes of the carbon cycle must improve considerably if we are to reliably identify carbon sinks/sources and to predict accurately the response of vegetation to climate change.

How can we account for the uncertainty in global estimates of primary productivity? Firstly, no direct measurements ("truth") exist for global NPP or GPP (Anav et al 2015). Secondly, the process-based land-surface and carbon models, which are frequently used for estimation, vary in their representation of mechanisms which are not completely understood (e.g. stomatal conductance, soil water dependence, leaf biochemistry; Knorr & Heimann 2001; Cramer et al 2001; Baker et al 2008; Bonan et al 2011). Thirdly, many of these models are over-parameterised with respect to the number of observable quantities available for either assignment or model calibration (Medlyn et al 2005; Zaehle et al 2005; Friend et al 2007; Prentice et al 2015). Fourthly, measurement or inference of NPP and GPP at site level, which is then used for global upscaling or model calibration, is subject to significant (∼20%) bias e.g. a preponderance of carbon sinks and lack of closure at FLUXNET sites (Wilson et al 2002; Baldocchi 2008), and systematic underestimation of NPP owing to frequently unmeasured below-ground productivity (Clark et al 2001; Malhi et al 2011).

Another reason why global estimation is challenging – one that has received less attention in the past – is that the sampling at site level is sparse and with an uneven geographical distribution. That several PFTs are undersampled *numerically*, by FLUXNET for example, is noted by several previous authors. For example, Beer et al (2010) highlight inadequate coverage of C4 vegetation in their estimates of global GPP based on an ensemble of land-surface and statistical models. In proportion to global vegetation, Alton (2013) notes a dearth of tropical broadleaf forests and C4 grasslands. Indeed, a review by Schimel et al (2015) reveals that 85% FLUXNET sites are located between 30-50°N and that coverage is severely limited in two critical "tipping regions" for positive feedbacks of the carbon cycle: the tropics and latitudes ≥60°N. That certain geographical regions are devoid of FLUXNET towers is also noted (e. g. India; Sundareshwar et al 2007).

Whilst undersampling of certain vegetation types is generally recognised, what is less clear is whether carbon-monitoring sites are typical, in terms of climate and canopy density, of the global PFTs they are intended to represent. With respect to canopy density, Baret et al (2006) note undersampling of sparse vegetation by networks such as FLUXNET. Systematic differences in carbon balance occur for forest canopies in different stages of development after disturbance (de Lucia et al 2007; Amiro et al 2010) but the distribution of sampling for different canopy densities within the same global PFT has rarely been analysed. With respect to climate, Xiao et al (2012) surmised that "FLUXNET is fairly representative of major climate types". However, this hypothesis has seldom been tested in a quantitative manner at global level. At regional level, Hargrove et al (2003) conclude that the representativeness by Ameriflux sites of mainland USA ecoregions (defined by climate and edaphic properties) is robust for all but marginal areas of the continent. Yang et al (2008) concur using remotely sensed quantities for both climate and vegetation density. Using similar quantities, He et al (2015) find that the representativeness of FLUXNET sites in China is good for croplands and grassland but rather poor for sparsely vegetated areas. Sulkava et al (2011) adopt a similar approach to Hargrove et al (2003) to analyse representativeness within Europe. Globally, there appears to be only a single study of the representativeness of FLUXNET (Kumar et al 2016) where multivariate clustering of climatic and edaphic variables is used to define ecoregions and then determine the proximity of the next-nearest FLUXNET site to these ecoregions. The authors infer that representativeness is high except for the tropics. We emphasise that previous studies use a single (next-nearest) FLUXNET site to determine how well a region is represented. There is potential, however, to average across all sites of the corresponding vegetation type to produce a more robust measure of representativeness. This is because any empirical upscaling of primary productivity, or use of carbon models calibrated for this purpose, would preferentially make use of the maximum number of available sites.

The recent release of a standardised GPP dataset (FLUXNET2015) provides an opportunity to re-examine the issue of representativeness for eddy covariance sites. A database of a similar size (EMDI), which has received little focus in the past, permits the same exercise for site NPP. The EMDI database was compiled to provide reliable (above and below ground) measurements for calibration of global LSMs but its ability to represent global vegetation has never been assessed. We determine the ability of these two primary carbon-monitoring networks to represent global vegetation by calculating the euclidian distance in climate-canopy space between global 0.5° cells and all sites of the same PFT. We believe that averaging across all sites, rather than calculating proximity to a single (next-nearest) location, procures a more robust measure of representativeness. We then upscale the cells to PFT and global levels, using site values of GPP and NPP and the inverse euclidian distances as weights. We do this in order to ascertain the importance of each vegetation type to global primary productivity (both GPP and NPP) in the context of how well each PFT is currently sampled. Kumar et al (2016) conduct global upscaling of GPP over ecoregions, rather than PFTs, using an inverse weighting similar to our own. However, they focus on temporal (seasonal and interannual) patterns, rather than on spatial annual averages as we do here. Similarly, Chu et al (2017) also investigate the temporal evolution of representativeness across FLUXNET. Representativeness has also been examined, to some extent, with complex statistical upscaling models in order to determine the ability of these models to extrapolate into environments that have not been used for model calibration (Jung et al 2009; Papale et al 2015).

The specific research questions of the current study are as follows:

1. How well are the major PFT contributors to global primary productivity currently represented in carbon-monitoring networks?;
2. Do networks used for upscaling (and carbon-model calibration), such as FLUXNET2015 and EMDI, provide a robust representation of global vegetation? If not, which global climate zones and canopy densities require better representation and how many sites should we sample to 'usefully' quantify primary productivity of the land carbon cycle?
3. What is the dispersion in NPP and GPP for sites of the same PFT and what uncertainty does this dispersion engender in undersampled PFTs and upscaled estimates of global primary productivity?
4. How do our upscaled estimates of global GPP and NPP compare with recent (mostly model-based) estimates?

3 Materials and Methods

The Methods are organised into five major sections. Firstly, we define representativeness and discuss the variables required to calculate it (§3.1). Secondly, we describe a straightforward upscaling, based on these variables, to determine the contribution, and therefore importance, of each PFT to global primary productivity (§3.2). Thirdly, we introduce the datasets required for global cells (§3.3). Fourthly, we discuss the carbon-monitoring networks and the datasets they provide for primary productivity (§3.4). Lastly, we summarise the workflow and discuss sources of error and ways to enhance representativeness (§3.5).

3.1 Determining Representativeness

For each 0.5° vegetated global landpoint cell, we calculate the inverse euclidian distance (w_i) in environmental variable space (var) between the global cell (var_{cell}) and a carbon-monitoring site (i) of the same PFT (var_i). Thus:

$$w_i = \frac{1}{\sqrt{\sum_{var} \left(\frac{var_{cell} - var_i}{sd(var)} \right)^2}} \tag{1}$$

Here, $sd(var)$ is the standard deviation of the environmental variable, var, from the mean across all global cells of the corresponding PFT. Dividing by $sd(var)$ normalises the euclidean distance, allowing us to incorporate variables of quite different ranges. We define climate zone using the primary climatic variables of temperature, precipitation and shortwave radiation (Strahler & Strahler 2013; Schimel et al 2015). However, we also take some account of differences in canopy cover within the same PFT by incorporating Leaf Area Index (LAI). Therefore, we define environmental variable space using Mean Annual Temperature (MAT; °C), Mean Annual Precipitation (MAP; mm yr^{-1}), Mean Annual Shortwave Radiation (MASW; W m^{-2}) and the mean average of maximum seasonal LAI ($\overline{LAI}_{max}$; $m^2 m^{-2}$). To evaluate Eq. 1 we require MAT, MAP, MASW and $\overline{LAI}_{max}$ (hereafter 'climate-canopy space') for all global cells (§3.3 below) and for all carbon-monitoring sites (§3.4 below).

In Eq. 1, w_i indicates the inverse euclidian distance in climate-canopy space separating the global cell from an individual carbon-monitoring site of the same PFT. To evaluate how well the global cell is represented by all corresponding carbon-monitoring sites, we define a modified mean inverse distance for each global cell (w_{cell}) by averaging over w_i thus:

$$w_{cell} = \frac{n_{var} \sum_{i=1}^{n} w_i}{2n} \tag{2}$$

where n_{var} is the number of environmental variables (i.e. 4) and n is the number of sites for this PFT. We group and average w_{cell} for global cells of the same PFT to determine how well each global PFT is represented overall by carbon-monitoring sites (w_{pft}). For random (non-biassed) sampling of the global PFT we expect $w_{cell} \simeq 1$. We also create global maps of w_{cell} to identify regions which are well/poorly represented. Note that w_i, w_{cell} and w_{pft} are calculated separately for each carbon-monitoring network.

The use of inverse euclidian distance is fairly well established as a means of defining proximity in environmental variable space (e.g. Hargrove et al 2003; Kumar et al 2016). Use of squared ($\propto w_i^2$), rather than linear ($\propto w_i$), weighting produces an oversensitivity both to the normalisation of the variable (sd(var) in Eq. 1) and to a small number of (the very closest) sites.

3.2 Weighted Upscaling

To determine the contribution, and therefore importance, of each PFT to global primary productivity, we conduct a straightforward upscaling of fluxes from carbon-monitoring sites to global level. The carbon flux (NPP or GPP) at each global cell (F_{cell}) is approximated by the weighted mean of the annual carbon flux measured at all relevant carbon-monitoring sites (F_i). Thus:

$$F_{cell} = \frac{\sum_{i=1}^{n} w_i F_i}{\sum_{i=1}^{n} w_i} \tag{3}$$

where relevant sites (i=1,n) are those comprising the network in question (EMDI for NPP and FLUXNET2015 for GPP) and are of the same PFT as the global cell. The weights, w_i (hence nomenclature), follow from Eq. 1. F_{cell} is subsequently integrated to PFT and global levels.

We recognise that this upscaling is simple compared to process-based and statistical models but it has the advantage of using environmental variables that are readily available both globally and at site level. The environmental variables (temperature, precipitation, shortwave radiation and leaf cover) have a first order influence on photosynthesis (e.g. Field et al 1995; Waring & Running 1998; Nemani et al 2003; Gurevitch et al 2006). Ideally, soil water availability might replace precipitation for the upscaling but this is a derived, rather than observed, variable requiring a water-balance model and knowledge of soil properties (e.g. Sellers et al 1997; Zhao & Running 2009). Such soil properties are undocumented for EMDI sites and many of the FLUXNET sites. Nearly half of the PFTs within FLUXNET2015 have sample sizes of $\leq$5 and this constraint on the number of degrees of freedom explains our predilection for a small number (4) of environmental variables.

3.3 Global Cells

To characterise the climate for the global cells in Eq. 1, we adopt the 3 hr reanalysis meteorology from Princeton University (Sheffield et al 2006; 2012; hereafter "Princeton meteorology"), which is reconstructed globally at 0.5° spatial resolution. Annual averages for MAT, MAP and MASW are created over the 7 yr period 2002-2008 (incl.), which corresponds to the overlap period with global LAI from MODIS.

Global LAI maps at 0.5° resolution are created for 2002-2008 (incl.) by extracting and mean averaging 0.5 km pixels in the standard 8-day MCD15A2H (C6) MODIS product. The latest C6 LAI product corrects for long-term detector degradation present in previous (e.g. C4 and C5) releases (Yan et al 2016; Zhang et al 2017a). Only pixels of good quality are selected i.e. main algorithm, no significant cloud and >50% detectors working (Yang et al 2006b). To minimise noise in the phenology timeseries to be created (De Kauwe et al 2011), the global 0.5° maps are averaged temporally using a median 32-day moving window, except for the tropics where persistent cloud (Zhao et al 2005) necessitates selection of the maximum LAI value over a moving 48-day window (Ryu et al 2011). For each global 0.5° cell, we extract the maximum LAI in each year and mean-average these values to produce $\overline{LAI}_{max}$.

PFT classification for each global cell is determined by the dominant landcover in the HYDE database (Goldwijk et al 2011) which provides a 0.5° global landcover map at the year 1990 (Fig. 1). Each cell is assigned to one of the PFTs in Tab. 2. The adopted PFTs are based on the land-surface model JULES-SF, which has been calibrated against FLUXNET sites in the past (Alton 2016; Alton 2017), and for which a sister paper is in preparation, assessing the impact of representativeness on model calibration. Various sources exist for landcover (e.g. Loveland et al 2000; Hansen & Reed 2000) but Goldwijk et al distinguishes carefully between natural and anthropogenic (pasture and cultivation) landcover. To distinguish cells dominated by C_3 grasses/crops from those dominated by C_4 grasses/crops, we use the global map of Still et al (2003) which quantifies the fraction of C_4 vegetation in each grid-cell.

3.4 Carbon-monitoring Networks

We adopt two carbon-monitoring networks: (1) FLUXNET2015 where GPP is inferred from tower-based eddy-covariance measurements; and (2) EMDI where annual NPP is measured through field sampling. These measurements are discussed in turn below along with their adopted meteorology and LAI data.

3.4.1 FLUXNET2015

FLUXNET2015 tier 1 (http://fluxnet. fluxdata. org) provides a harmonised database of 151 sites covering a range of PFTs made freely available to the modelling community. High-quality fluxes, including net ecosystem exchange, are inferred from eddy covariance. The measurement timestep is either 30 mins or hourly. Measurements are gap-filled, using a well-tested standardised method (Reichstein et al 2005), when data are either missing or recorded under low friction velocity (insufficient turbulence; Barr et al 2013). Two standard products for GPP are available with FLUXNET2015: (1) an empirical temperature fit to nighttime respiration which is extrapolated to daytime in order to subtract daytime respiration from net ecosystem exchange to yield GPP (gpp_nt_ref; Reichstein et al 2005); and (2) an empirical fit of daytime net ecosystem exchange against downwelling shortwave radation to infer daytime respiration at zero irradiance which can then be subtracted from daytime net ecosystem exchange to yield GPP (gpp_dt_ref; Lasslop et al 2010). A site list, with site coordinates, principal investigators, citations and general description is provided at http://fluxnet.fluxdata.org and is also summarized by Haughton et al (2018). The geographical distribution, discussed in the Results, is also shown in Fig. 7. Siteyears span 1991-2014 but the mean year and standard deviation for the dataset are 2007±5.

We summed the (half-)hourly values of both gpp_dt_ref and gpp_nt_ref to produce average annual GPP over the siteyears available at each site (7 on average). The root mean square difference between the two estimates was <1% which is small compared to the other sources of error (discussed below). Therefore, we adopted gpp_dt_ref as the measured site GPP. (Half-)hourly *in situ* meteorology, recorded by the fluxtower instruments, is averaged over all siteyears available for each site to determine MAT, MAP and MASW. Note that we sum to *annual* values of GPP for consistency with EMDI which only provides annual values of NPP.

To create an LAI 2002-2008 timeseries for each carbon-monitoring site, we follow the procedure above for global cells but extract a 3.5 km × 3.5 km subset (49 pixels) centred on the site. Note that subsets smaller than this are considered less robust in terms of the LAI produced by the MODIS radiative-transfer algorithm (Yang et al 2006a; Yang et al 2006b; Heinsch et al 2006). For each site, we extract the maximum LAI in each year and mean-average these to produce $\overline{LAI}_{max}$.

3.4.2 EMDI

EMDI is a standardised database for field-based annual NPP divided into class A (well-documented) and class B (less well-documented) sites (Olson et al 2008). The revised (R2) version of these datasets was accessed from the Land Processes Distributed Active Archive Center (LP DAAC) at the website daac. ornl. gov/NPP. Initially, we only used sites where both aboveground and belowground NPP were measured, yielding a total of 306 sites. Of these sites, ≃10% have repeat measurements and these repeat values were mean-averaged to yield NPP measurements for 277 sites. This approach led to very small sample sizes in some PFTs. Therefore, the requirement for belowground NPP to be measured was relaxed for C3 and C4 crops, savanna, tundra shrubs and non-tundra shrubs. Where belowground NPP is absent, the EMDI database assumes a value of one for the aboveground-to-belowground NPP ratio for these PFTs (Olson et al 2008). Some previous studies adopt a larger number of class B sites from the EMDI database and rely, therefore, more heavily on the assumed ratio of aboveground-to-belowground NPP (e.g. Zaks et al 2007). However, we prefer to use a smaller, more robust, set of measurements which is comparable in size to the FLUXNET2015 database and makes less reliance on this ratio.

In lieu of an *in situ* meteorology for EMDI sites, we adopt the Princeton meteorology, using bi-linear interpolation across the four 0.5° global cells closest in longitude and latitude to the site in question. Zaks et al (2007) use reanalysis meteorology at 10 arcmin resolution for EMDI sites but disaggregation to this spatial resolution entails greater uncertainties in the resultant meteorology. To test the impact of using a 0.5° (rather than *in situ*) meteorology, we conduct a separate experiment in which we substitute the tower-based meteorology at FLUXNET2015 sites with the interpolated Princeton meteorology and monitor the change in representativenss for GPP. To determine $\overline{LAI}_{max}$ at EMDI sites, we proceed as above for FLUXNET2015 (§3.4.1).

3.5 Workflow, Error Analysis and Enhancing Representativeness

3.5.1 Workflow

We substitute values of MAT, MAP, MASW and $\overline{LAI}_{max}$ for both carbon-monitoring sites and 0.5° global grid cells into eq. 1. The standard deviation of each environmental variable, across global cells of the same PFT, is also evaluated and substituted. We derive w_{cell} from Eq. 2 as a measure of representativeness for each global cell. Using Eq. 3, both NPP and GPP are summed for each cell to produce totals at PFT and global levels.

3.5.2 Error Analysis

Random errors in annual carbon fluxes at FLUXNET sites are estimated at only 5% (Hollinger & Richardson 2005; Baldocchi 2008). For annual GPP, the combined random uncertainties, including gap-filling, are estimated at <10% by Beer et al (2007). Comparing the root-mean-square difference between duplicate measurements within the EMDI database (available for 10% of sites; n=29), we infer a random error of 15% in site NPP. Systematic errors are larger than random errors for both NPP and GPP but it is difficult to account for them in their overall effect. Poor detection of high frequency gas fluctuations leads to systematic underestimation by 5-10% (Baldocchi 2008). However, incomplete energy closure suggests that underestimation might be larger (20%; Wilson et al 2002). Incomplete sampling of components (e.g. herbivory, smaller trees in plots) suggests a systematic underestimation of at least 20% in field-based NPP (Clark et al 2001; Malhi et al 2011). Whilst systematic errors probably lead to underestimation of both GPP and NPP, the vast majority of FLUXNET sites are known to be carbon sinks (Baldocchi 2008; Amiro et al 2010) and these sites, therefore, may be more productive than the global PFT they represent.

For historical reasons, mostly concerned with accessibility and funding, both carbon-monitoring networks undersample numerically certain vegetation types. To account to some extent for limited sampling and random errors, we adopt a bootstrap method in our upscaling by randomly selecting site measurements with replacement (10000 iterations for both EMDI and FLUXNET2015) and monitoring the variation in PFT-level and global estimates (standard deviation from the mean).

3.5.3 Enhancing Representativeness

To quantify the number of sites needed to sample each global PFT accurately we conduct a separate, additional experiment for upscaling. We reduce the number of sites for PFTs which are numerically well represented so that they approach the sample size of those PFTs which are the least well represented numerically. This is done using random selection without replacement for sample sizes of 48, 24, 12, 6, and 3, where the starting point (48 in this example) is the maximum number of sites available for the well-represented PFT in question. Estimation of GPP and NPP at PFT level is monitored as the sample size changes (mean and standard deviation over 1000 iterations for each sample size).

The above approach assumes that carbon-monitoring sites are distributed evenly in climate-canopy space. However, the global PFT may occupy large areas of climate-canopy space which are not sampled at all at site level. Furthermore, our estimates of PFT primary productivity rely on *interpolating* between sites across climate-canopy space since they depend on a weighted upscaling (Eq. 3). To estimate the fraction of primary productivity which lies outside of the sampled climate-canopy space we employ a state-of-the-art

land-surface model (JULES-SF) which has previously been calibrated against diverse carbon flux datasets (Alton 2013).
JULES-SF (Joint UK Land Environmental Simulator) is an enhanced version of the new UK Met. Office Surface Exchange Scheme (Cox et al 1999). It is state-of-the-art for ecophysiological process-based global models of the Penman-Monteith type (Monteith 1965) but represents particularly well multilayer light interception and photosynthesis within the canopy (Alton & Bodin 2010; Alton 2016). Note that we are not using this particular model to validate the upscaled values (i. e. as "truth") since models vary in their inherent assumptions as well as their estimates of PFT and global primary productivity (Ito 2011; Anav et al 2015; Prentice et al 2015). However, we assume that the model provides a useful surrogate for truth (Jung et al 2009) since it fully samples climate-canopy space for each PFT and *may*, therefore, indicate how primary productivity varies systematically between the interpolated and extrapolated climate-canopy space. To this end, we define a ratio for both GPP and NPP which is the model estimate for the interpolated climate-canopy space divided by the estimate for the full global climate-canopy space. We define the interpolated climate-canopy space as mean ± 2 standard deviations across all 4 environmental variables where the mean and standard deviation correspond to FLUXNET2015 and EMDI sites, respectively, for GPP and NPP. The model provides an estimate of GPP and NPP for all global $0.5°$ landpoints which reside within this mean ± 2 standard deviations climate-canopy space as well as across the full global climate-canopy space. The interpolated space is defined generously (using 2 standard deviations) and, therefore, provides a lower limit to any biases which are detected.

4 Results and Discussion

To ascertain which PFTs are important contributors to global primary productivity, we first analyse the upscaling (§4.1) before examining the representativeness of the carbon-monitoring networks themselves (§4.2). Next, we investigate how many sites are required for the network to be representative of global PFTs (§4.3). The final section (§4.4) treats the limitations and caveats to the study.

4.1 Upscaling

Our weighted upscaling yields 131 ± 8 Gt yr^{-1} and 66 ± 4 Gt yr^{-1} for annual global GPP and NPP, respectively. Uncertainties follow from our bootstrap error analysis but, as noted above, this does not account for systematic errors associated with the site fluxes (EMDI and FLUXNET2015) used for upscaling. Global Carbon-Use Efficiency (NPP/GPP) is 0.50 ± 0.04, which is close to the value prescribed in many carbon models (e.g. Waring et al 1998).

There are no measurements of GPP and NPP at global level that would serve for validation purposes (Anav et al 2015). However, given the simplicity of the method, our upscaled values compare fairly favourably with a compilation of previous estimates based on a diversity of methods (Tab. 3). Thus, our global NPP (66 ± 4 Gt yr^{-1}) lies at the upper end of 251 previous estimates compiled by Ito (2011) and averaged according to method (46-61 Gt yr^{-1}). Note, however, that this previously inferred range conceals a large standard deviation (13 Gt yr^{-1}) between studies using a similar technique. Recent estimates might be converging towards a value of 56 ± 14 Gt yr^{-1} (Ito 2011) but they also rely increasingly on models which contain numerous parameters, some of which are poorly constrained (Prentice et al 2015). Compared to NPP, far fewer global estimates of GPP are available. Recent estimates tend towards lower values (110-120 Gt yr^{-1}), possibly owing to a greater reliance on Light-Use Efficiency models, including the standard MODIS products of GPP. Both ecophysiological process-based models and top-down studies of atmospheric isotopes still allow for a broad range of global GPP and, indeed, much higher values (≤ 175 Gt yr^{-1}). Our estimate (131 ± 8 Gt yr^{-1}) is fairly central with respect to previous estimates.

The three PFTs which contribute most to global GPP are tropical broadleaf forest, non-mediterranean neeedleleaf forest and C3 grass (collectively 64%; Tab. 4). This is 9% higher than Beer et al (2010), who collate several (mostly model-based) estimates but find that productivity is higher in C4 (tropical) grassland compared to C3 (temperate) grassland (an inference which depends on the adopted global landcover). For NPP, Tab. 4 reveals a similar situation to GPP, except that the biggest single contributor is C3 crop (26% global NPP). The accuracy of NPP estimates for this PFT is discussed below (§4.3).

4.2 Site Representativeness

Focussing initially on site numbers, we show the proportion of each carbon-monitoring network distributed over each PFT and compare to the corresponding percentage of global area for that vegetation type (Tab. 2). For historical and accessibility reasons, both networks over-represent non-tropical (temperate) broadleaf forest by an order of magnitude. This is in spite of the modest contribution of this PFT to global NPP and GPP (2-3% in Tab. 4). Tropical broadleaf forest is under-sampled by FLUXNET2015, even though this PFT contributes 29% to global GPP (Tab. 4) and is poorly constrained as a carbon sink/source (Gurney et al 2002). The observation that FLUXNET undersamples tropical forest and oversamples temperate forests is noted by previous authors (e.g.Schimel et al 2015) but here we quantify in proportion to global land-surface (see also Baret et al 2006) and place in the context of the relative contributions of each PFT to global primary productivity.

Fig. 2 compares the distribution of both carbon-monitoring networks with global vegetated 0.5° cells in terms of climate, specifically MAP and MAT. This graph confirms an undersampling of tropical rain forest within FLUXNET2015 (MAP>2500 mm yr^{-1}, MAT>25°C). Both networks undersample warm and cold (semi-)arid climes (MAP<400 mm yr^{-1}), even though some of these regions are subject to the greatest climate change and perturbation to their carbon cycle (e. g. warming/greening of the northern tundra; Myneni et al 1997; Elmendorf et al 2012).

The sampling density within MAP-MAT climate space is quantified in Fig. 3 and compared with global vegetated cells. Outliers confirm over-representation (by a factor 2-3) of woodland, shrubs and forest within temperate regions (MAP=750 mm yr^{-1}, MAT=5-15°C) using the idealised climate-biomes of Whittaker (Fig. 2). In contrast, there is a dearth of sites within the tundra (MAP=250 mm yr^{-1}, MAT=-15°C). The pronounced scatter in panel (b) of Fig. 3 (R^2=0.17-0.20) reveals that both networks are mediocre in their representation of global MAT-MAP space, although the strengths and weaknesses of each network vary according to PFT.

(Semi-)arid regions are poorly sampled in Fig. 2 (both warm and cold). Furthermore, of the vegetated global cells with MAP<400 mm yr^{-1}, 91% correspond to sparse vegetation with $\overline{LAI}_{max} \leq 2$ m^2m^{-2}. On average, $\overline{LAI}_{max}$=0.97 m^2m^{-2} for global vegetated cells with MAP<400 mm yr^{-1} compared to $\overline{LAI}_{max} = 3.0$ m^2m^{-2} for MAP≥400 mm yr^{-1}. Fig. 4 reveals how carbon-monitoring networks represent global vegetation in terms of LAI. Notably, 50% global vegetation is characterised by $\overline{LAI}_{max} \leq 2$ m^2m^{-2} but only 30-32% of both networks sample vegetation with an LAI as low as this. We estimate from our global upscaling that 0.5° cells with $\overline{LAI}_{max} \leq 2$ m^2m^{-2} contribute 31% global GPP and 35% global NPP. The situation is more acute at lower canopy densities. Thus, 25% of the vegetated land-surface possesses $\overline{LAI}_{max} \leq 1$ m^2m^{-2} but only 10% network sites sample such sparse vegetation. This dearth is noted when networks such as AERONET or FLUXNET are used to validate global satellite products (Baret et al 2006).

For certain PFTs, the corresponding sites are relatively numerous but those sites fail to sample the average global climate of the PFT they represent. This is seen in Fig. 5 where the modified mean inverse euclidian distance (w_{pft}) for global cells containing mediterranean needleleaf is lower than other PFTs (poor representativeness). This is in spite of relatively high site numbers for this PFT in both networks (Tab. 2). On average, MAP and MAT are higher within the combined site samples of FLUXNET2015 and EMDI for mediterranean needleleaf (1210 mm yr^{-1} and 13.5°C, respectively) compared to the mean values of the corresponding global cells (550 mm yr^{-1} and 1.7°C). Similarly, non-tundra shrubs are sampled in the mid-latitudes (mean absolute latitude 40°), whilst the global distribution is weighted more towards the sub-tropics (mean absolute latitude 22°; panel (a) of Fig. 6). This bias results in a low value of w_{pft} in Fig. 5, particularly with respect to FLUXNET2015.

In terms of climate-canopy space, Figs. 7 and 8 reveal which parts of the globe are well represented by FLUXNET2015 and EMDI, respectively, by mapping the modified mean inverse euclidian distance (w_i in Eq. 2). Superimposed markers for site locations reveal the pronounced clustering of carbon-monitoring sites within Europe and North America. The poor representativeness of tropical broadleaf forest, discussed above, is particularly conspicuous for the Old World formations in Africa and south-east Asia, especially for FLUXNET2015. This is already noted for south-east Asia by Kumar et al (2016), who assess global representativeness of FLUXNET with a next-nearest approach. Figs. 7 and 8 also reveal that both networks represent rather poorly the northern half of the boreal conifer belt owing to site sampling of non-mediterranean needleleaf forest at lower latitudes (compare with landcover in Fig. 1 and see panel (b) of Fig. 6). Note that some regions have high representativeness in Figs. 7 and 8, even though they contain few carbon-monitoring sites. This is due to their proximity in climate-canopy space to sites of the same vegetation located elsewhere in the world. Thus, in West Asia, both C3 grassland and C3 crops have high representativeness for, respectively, NPP and GPP owing to sampling in, respectively, Europe and North America.

The global distribution of NPP sampling has received very little attention in the past and Fig. 8 constitutes, to our knowledge, the first assessment of representativeness by EMDI. This network compiles NPP measurements for well-studied sites with the stated aim of improving global carbon models (Olson et al 2008). EMDI combines geographically dispersed measurements from the literature with previously collated databases, the latter often compiled for a specific purpose (e.g. change in forest NPP along a transect). As with FLUXNET2015, measurements are biassed towards regions with better access and resources. Note, however, that the S. American tropical broadleaf forest is better represented by EMDI compared to FLUXNET2015 (Figs. 7 & 8). C3 grasslands are also better represented, owing to inclusion of an intensive study by Gill et al (2002), but C3 crops are better sampled by FLUXNET2015.

Tab. 5 quantifies the climate-canopy distribution of global cells compared to the carbon-monitoring networks by presenting the mean and standard deviation of each environmental variable according to PFT. The tabular data confirm that certain PFTs (e.g. non-mediterranean needleleaf forest, mediterranean needleleaf forest and tundra) are sampled, by either one or both carbon-monitoring networks, in more temperate (wetter and warmer) climes compared to their global distribution (see panel (b) of Fig. 6 for non-mediterranean needleleaf forest). Similarly, the table confirms the inference drawn from Fig. 6, namely, that non-tundra shrub is generally sampled in cooler regions compared to its principally sub-tropical global distribution. A similar conclusion is drawn for C4 crops from Tab. 5. Some of these PFTs (C4 crops and non-tundra shrub) only make a small (1-2%) contribution to global primary productivity. However, non-mediterranean needleleaf forest contributes, respectively, 13% and 17% to global NPP and global GPP in Tab. 4. The global centroid of this PFT is -3.9±5.4°C, 510±270 mm yr^{-1}. This overlaps greatly with the Whittaker climate-biome designated as “tundra” in Fig. 2, previously noted as relatively devoid of sampling sites. As stated in connection with Fig.4, 50% vegetated global cells have $\overline{LAI}_{max} \leq 2$ m^{2}m^{-2}. Of these sparsely vegetated global cells, 25% are classified as non-mediterranean needleleaf forest and 17% as tundra shrub. Therefore, better sampling of the climate-canopy space of these PFTs, especially non-mediterranean needleleaf forest, is important. The bias towards more temperate needleleaf sites, which are possibly more productive than the majority of the boreal needleleaf forest (owing to a more clement climate and higher LAI; Tab. 5), may explain why some land-surface models, when calibrated against FLUXNET sites, underestimate continental runoff at high northern latitudes (Alton 2013) compared to measured river-mouth discharge (Dai et al 2009). The deficit in runoff suggests an overestimation of evapotranspiration, which is frequently dominated by transpiration for the vegetated land-surface (Jasechko et al 2013). Transpiration itself is tightly linked to GPP through stomatal conductance and this physiological link is exploited in regional and global estimates of GPP based on water-use efficiency (Beer et al 2007; 2010).

4.3 Enhancing Representativeness: How many sites are required?

The number of sites required to sample carbon fluxes fully depends not only on the distribution of global climate-canopy space, as discussed above, but also on the range in primary productivity measured across sites of the same PFT. We begin by focussing on this latter issue, which has received little discussion in the literature, before estimating how many sites are required.

Barcharts for site GPP and NPP, expressed in kg m^{-2} yr^{-1} and grouped by PFT, exhibit a large spread (Fig. 9). Indeed, averaging across all PFTs for both NPP and GPP, the standard deviation in primary productivity constitutes 56% mean. It is this broad range in Fig. 9 that leads to substantial uncertainties in PFT primary productivity in Tab. 4 (on average 18%, but up to 40% for some PFTs). This is because a large number of sites must be sampled to provide precise estimates of the primary productivity of each PFT. For NPP in Fig. 9, our PFT means are close (root mean square difference of 0.13 kg m^{-2} yr^{-1}) to those derived from previously compiled field measurements (Houghton & Skole 1990) when excluding crops (discussed below). They are also very close (root mean square difference of 0.09 kg m^{-2} yr^{-1}) to the means estimated by Luyssaert et al (2007) for forest PFTs. These authors collate both NPP and GPP from diverse methods including eddy covariance, leaf chamber, harvesting, allometry and process-based models. For GPP in forests, our PFT means are fairly close (root mean square difference of 0.22 kg m^{-2} yr^{-1}) to those of Luyssaert et al (2007) when omitting tropical broadleaf forest. Our mean GPP for tropical broadleaf forest (2.4 kg m^{-2} yr^{-1}) is lower than that of Luyssaert et al (3.6 kg m^{-2} yr^{-1}) but within 20% of the mean of 13 tropical forests (2.9 kg m^{-2} yr^{-1}) compiled by Fu et al (2018). Site NPP for C3 crops in Fig. 9 exhibits a very wide range (0.8-2.0 kg m^{-2} yr^{-1}) compared to other PFTs and is higher, on average, than more recent estimates (0.5-1.0 kg m^{-2} yr^{-1}; Ciais et al 2010; Li et al 2014). The CUE (ratio NPP/GPP) also appears too high in Fig. 9 compared to the theoretical and previously observed upper limit of 0.7 for non-woody vegetation (Choudhury 2000; van Iersel 2003). Measured crop NPP appears to vary greatly according to both species and treatment (irrigation and fertiliser) within the EMDI database. If this network generally overestimates for this PFT, the corresponding contribution to global NPP (26%; Tab. 4) may be too high (perhaps by a factor 2).

We determine the number of sites required to quantify precisely the productivity of each PFT. As explained in §3.5.2, we do this by reducing the number of sites used in the upscaling. We do this for PFTs which are numerically well represented (i. e. non-tropical broadleaf forest and C4 grassland for NPP, and non-mediterreanean needleleaf forest and C3 grassland for GPP) so that they approach the sample size of PFTs which are the least well represented numerically. For those PFTs in Tab. 2 with few (2-6) site samples (e.g. C4 crop), this bootstrap uncertainty analysis suggests that errors in NPP and GPP are large (20-40%; see Fig. 10). Furthermore, we require 30 and 50 sites per PFT to estimate PFT productivity to, respectively, 5% and 2% precision. Undersampling of individual PFTs has less impact globally owing to cancellation when integrating from PFT to global level (6% for both global NPP and GPP; see uncertainties in bottom row of Tab. 4). However, to be able to quantify and to monitor carbon-sinks within individual PFTs as a percentage of anthropogenic CO_2 release (9 Gt yr^{-1} or 10-15% global NPP; Le Quéré et al 2015), we seek a precision of at least 2% at PFT-level. This requires a carbon-monitoring network consisting of at least 600 (50×12 PFTs) sites which are carefully selected (see below) to represent adequately the climate-canopy space of global vegetation. Using a complex statistical model (artificial neural network) to upscale GPP for Europe, Papale et al (2015) recognise a stablisation in the inferred values when incorporating more than 30-50 FLUXNET sites into the model calibration. Although this study pools sites from different PFTs, it appears that the resulting stability (we infer $<5\%$ from their Fig. 3) is consistent with the results in Fig. 10.

Our estimates of the number of required sites per PFT must be considered as a minimum. The bootstrap assumes a random set of measurements across the global distribution. However, as discussed above, certain PFTs are sampled within the "wrong" latitude or climate and, as such, might be too clumped compared to the corresponding global range. This is demonstrated in Fig. 11 which indicates how primary productivity simulated by a land-surface model (JULES-SF) differs between the climate-canopy space sampled by FLUXNET2015 or EMDI i.e. the interpolated space (defined as mean $\pm$ 2 standard deviations for the corresponding carbon-monitoring sites) and the global climate-canopy space of the PFT in question (§3.5.3). On the basis of Fig. 11, the primary productivity of non-mediterranean needleleaf forest (as a global PFT) may be overestimated by 20-30% owing to site sampling in relatively temperate climes compared to the global distribution (§4.2). Of the other main PFTs contributing to global primary productivity, values for C3 grass might be underestimated, owing to sampling at sites which are somewhat cooler than the global distribution (Tab. 5). However, sites for C3 crops and tropical broadleaf forest appear representative of productivity across the corresponding global PFT. This is in spite of low site numbers for tropical broadleaf forest within FLUXNET2015 – an inference also made by Jung et al (2009) when comparing a complex statistical upscaling, based on model trees, against output from the LPJmL biosphere model. The mean absolute difference between the interpolated-to-full ratios in Fig. 11 and unity is 15% and 11% for NPP and GPP, respectively. This is more than the 2% precision identified in Fig. 10 for 50 sites. This implies that locating new sites in previously unsampled climate-canopy space may be more important than a simple increase in the number of sites (Baret et al 2006).

4.4 Caveats and Limitations

Our bootstrapping and sampling experiments conducted above cannot account for bias in site measurements, such as the systematic underestimation of site NPP in field measurements (Clark et al 2001; Malhi et al 2011) or a preponderance of carbon sinks at disturbed sites within FLUXNET2015 (Baldocchi 2008; Amiro et al 2010). As noted earlier (§3.5.2), systematic errors and bias can be substantial ($\sim$20%). Site measurements for NPP within the EMDI database are mostly from the 1970s or later. On the basis of FACE experiments (Ainsworth & Long 2005) and observed increasing atmospheric CO_2 concentration (Keeling et al 1996), we might expect an enhancement in site NPP of up to 8% by 2002-2008 (period used for global NPP upscaling).

In lieu of an *in situ* meteorology for EMDI sites, we substituted the Princeton meteorology in our weighted upscaling, interpolating across the 0.5° grid cells that coincide with the site locations (§3.4.2). However, our results appears to be fairly insensitive to the dataset used for site meteorology. Thus, when replacing the tower meteorology at FLUXNET2015 locations with the corresponding Princeton meteorology, the mean representativeness at PFT level (w_{pft}) drops by 0.05 on average. This is equivalent to 6% and does not significantly affect the ranking of PFTs in terms of representativeness. Systematic differences between tower and Princeton meteorology are 0.8°C, 4% and 2% for MAT, MAP and MASW, respectively (n=154). These offsets are small compared to the standard deviation of the same variables across global PFTs which are used to normalise the euclidian distance in Eq. 1 (e.g. 53% for MAP when averaging across all PFTs in Tab. 5). Similarly, although MAT, MAP, MASW and $\overline{LAI}_{max}$ are only calculated from a 7yr period (2002-2008) for global cells, the environmental variable with the greatest interannual variation (MAP) is estimated to a standard error of 14%. Once again, this is much less than the standard deviation across the global PFT (53%).

Some of our results are sensitive to landcover. Global landcover maps often manifest differences in classification, particularly over heterogeneous landscapes (Quaife et al 2008). Site descriptions of landcover can also vary and are partly subjective (De Kauwe et al 2011). These inconsistencies engender uncertainty since: (i) representativeness depends on the landcover adopted for each global cell and is calculated with respect to sites of the same (or very similar) vegetation type; (ii) precise attribution of global primary productivity to different vegetation types depends on the adopted global landcover. The potential mixing/confusion of landcover at sites may also spuriously increase the productivity range determined for each PFT (Fig. 9).

The method adopted for upscaling is very simple. However, its primary purpose is to determine broadly which PFTs contribute most to global primary productivity. The number of environmental variables used for representativeness and upscaling could be extended, once larger samples (more sites) are available for all PFTs. Additional variables, assuming they become available for all sites, could include soil properties, especially those influencing plant water availability, and seasonality of climate. We also note that the extended network of FLUXNET sites, LaThuile, for which harmonised datasets of GPP are not yet available, still contains many of the geographical and climate biases discussed above for FLUXNET2015. Thus, interpolating across the 0.5° Princeton meteorology grid cells that coincide with LaThuile locations, an update of the MAP-MAT sampling density within Fig. 2, still reveals 2σ oversampling in temperate regions and little improvement in site-to-global correlation (r^2=0.18 for LaThuile *versus* r^2=0.17 using FLUXNET2015).

5 Summary and Conclusions

We determine the ability of two important carbon-monitoring networks (FLUXNET2015 and EMDI) to represent global vegetation by calculating the euclidian distance in climate-canopy space between global 0.5° cells and carbon-monitoring sites of the same PFT. One of the carbon-monitoring networks, FLUXNET2015, constitutes a fairly new data release. Primary productivity for global cells is calculated as a weighted average of annual carbon flux from sites of the same PFT and the inverse euclidian distance as weights. Subsequent integration of global cells leads to estimates of GPP and NPP at PFT and global levels. The purpose of this upscaling is to determine broadly the main PFT contributing to annual global primary productivity with a view to improving their representativeness in carbon-monitoring networks. The main conclusions from this study are as follows:

1. Upscaled global NPP and global GPP are 66±4 Gt yr^{-1} and 131±8 Gt yr^{-1}, respectively. Given the simplicity of the upscaling method and the range in existing estimates, this is fairly close to (10-20% higher than) the majority of recent (mostly model-based) estimates.

2. Of the main contributors to global NPP and GPP: (i) tropical broadleaf forest is numerically underrepresented, particularly in the Old World by FLUXNET2015 (though the currently sampled climate-canopy space for this PFT may permit more robust upscaling compared to other vegetation types); (ii) C3 crops are sampled "correctly" in climate-canopy space but the global contribution of this PFT is uncertain owing to sensitivity of productivity to species and treatment; and (iii) site measurements of non-mediterranean needleleaf forest are relatively numerous but sampling occurs at the "wrong" latitude and climate with respect to the global stronghold of this PFT within the boreal forest. Poor sampling of global climate space also occurs for several other PFTs (mediterranean needleleaf forest, non-tundra shrub and C4 crops) but their contribution to global primary productivity is an order of magnitude less than that of non-mediterranean needleleaf forest. Considering its modest contribution globally (2-3% primary productivity), non-tropical (temperate) broadleaf forest is oversampled compared to other PFTs.

3. (Semi-)arid regions (MAP<400 mm yr^{-1}) are undersampled by both carbon-monitoring networks, particularly the tundra and northern half of the boreal needleleaf forest. Of global vegetated cells with MAP<400 mm yr^{-1}, 91% are characterised by sparse vegetation cover ($\overline{LAI}_{max} \leq 2$ m^{2}m^{-2}).

In general, sparse vegetation is poorly sampled by both networks even though it covers 50% of the vegetated land-surface and contributes one third of global NPP and global GPP.

4. Site-measured NPP and GPP exhibit a broad range within the same vegetation type (standard deviation is 56% mean). As a consequence of this broad range, our bootstrap error analysis indicates that at least 50 sites per PFT are required to quantify the primary productivity of each global vegetation type sufficiently well (2% precision) in order to identify its potential role as a sink of anthropogenic carbon (assuming ecosystem respiration is measured to the same precision). A land-surface model simulation of primary productivity within the network-sampled climate-canopy space, compared against productivity simulated for *global* climate-canopy space, underlines the importance of adding sites which considerably extend the environmental range over which a given PFT is being sampled.

Acknowledgements

This work used eddy covariance data acquired and shared by the FLUXNET community, including these networks: AmeriFlux, AfriFlux, AsiaFlux, CarboAfrica, CarboEuropeIP, CarboItaly, CarboMont, ChinaFlux, Fluxnet-Canada, GreenGrass, ICOS, KoFlux, LBA, NECC, OzFlux-TERN, TCOS-Siberia, and USCCC. The ERA-Interim reanalysis data are provided by ECMWF and processed by LSCE. The FLUXNET eddy covariance data processing and harmonization was carried out by the European Fluxes Database Cluster, AmeriFlux Management Project, and Fluxdata project of FLUXNET, with the support of CDIAC and ICOS Ecosystem Thematic Center, and the OzFlux, ChinaFlux

References

Ainsworth, E., Long, S. (2005) What have we learned from 15 years of free-air CO_2 enrichment (FACE)? A meta-analytic review of the responses of photosynthesis, canopy properties and plant production to rising CO_2. New Phytol., 165(2):351-71.

Alton, P. and Bodin, P. (2010) A comparative study of a multilayer and a productivity (light-use) efficiency land-surface model over different temporal scales *Agricultural and Forest Meteorology*, 150, 182-195

Alton, P. (2013) From site-level to global simulation: reconciling carbon, water and energy fluxes over different spatial scales using a process-based ecophysiological land-surface model *Agricultural and Forest Meteorology*, 176, 111-124

Alton P. (2016) The sensitivity of models of gross primary productivity to meteorological and leaf area forcing: a comparison between a Penman-Monteith ecophysiogical approach and the MODIS Light-Use Efficiency algorithm *Agricultural and Forest Meteorology*, 218-219, 11-14

Alton, P., (2017) Retrieval of seasonal Rubisco-limited photosynthetic capacity at global FLUXNET sites from hyperspectral satellite remote sensing:Impact on carbon modelling *Agricultural and Forest Meteorology*, 232, 74-88

Amiro, B., Barr, A., Barr, J., Black, T., Bracho, R., Brown, M., Chen, J., Clark, K., Davis, K., Desai,A., Dore, S., Engel, V., Fuentes, J., Goldstein, A., Goulden, M., Kolb, T., Lavigne, M., Law, B., Margolis, H., Martin, T., McCaughy, J., Misson, L., Montes-Helu, M., Noormets, A., Randerson, J., Starr, G., Xiao, J. (2010) Ecosystem carbon dioxide fluxes after disturbance in forests of North America *JGR* 115, G00K02

Anav, A., Friedlingstein, P., Beer, C., Ciais, P., Harper, A., Jones, C., Murray-Tortarolo, G., Papale, D., Parazoo, N., Peylin, P., Piao, S., Sitch, S., Viovy, N., Wiltshire, A., Zhao, M. (2015) Spatiotemporal patterns of terrestrial gross primary production: a review *Reviews of Geophysics*, 53, 785-818

Baker, I.T., Prihodko, L., Denning, A.S., Goulden, M., Miller, S., da Rocha, H.R., (2008) Seasonal drought stress in the Amazon: reconciling models and observations. *J.Geophys. Res.* 113, G00B01, doi:10.1029/2007JG000644.

Baldocchi, D. (2008) 'Breathing' of the terrestrial biosphere: lessons learned from a global network of carbon dioxide flux measurement systems *Aust.J.Botany*, 56, 1-26

Baret, F., Morissette, J., R. Fernandes, J. L. Champeaux, Ranga B. Myneni, J. Chen, Stephen Plummer, M. Weiss, C. Bacour, Sebastien Garrigues, and Jamie E. Nickeson, (2006) Evaluation of the representativeness of networks of sites for the global validation and inter-comparison of land biophysical products: Proposition of the CEOS-BELMANIP *IEEE Trans. Geosci. Rem. Sens.* 44,1-10

Barr, G, Richardson, A., Hollinger, D., Papale, D., 2013, Use of change-point detection for friction-velocity threshold evaluation in eddy-covariance studies *Agricultural and Forest Meteorology*, 171, 31-45

Beer, C., Reichstein, M., Ciais, P., Farquhar, G., Papale, D., (2007) Mean annual GPP of Europe derived from its water balance *Geophysical Research Letters*, 34, L05401

Beer, C., Reichstein, M., Tomelleri, E. (2010) Terrestrial gross carbon dioxide uptake: global distribution and covariation with climate *Science*, 329, 834-838

Bodesheim, P., Jung., M., Gans, F., Mahecha, M., Reichstein, M., (2018) Upscaled diurnal cycles of land-atmosphere fluxes: a new global half-hourly data product *Earth Syst.Sci.Data*, 10, 1327-1365

Bonan, G. B., P. J. Lawrence, K. W. Oleson, S. Levis, M. Jung, M. Reichstein, D. M. Lawrence, and S. C. Swenson (2011), Improving canopy processes in the Community Land Model version 4 (CLM4) using global flux fields empirically inferred from FLUXNET data, J. Geophys. Res., 116, G02014, doi:10.1029/2010JG001593.

Carvalhais, N., Reichstein, M., Collatz, G., Mahecha, M., Migliavacca, M., Neigh, C., Tomelleri, E., Benali, A., Papale, D., Seixas, J. (2010) Deciphering the components of regional net ecosystem fluxes following a bottom-up approach for the Iberian Peninsula *Biogeosciences*, 7, 3707-3729

Chen, M., Rafique, R., Asrar, G. (2017) Regional contribution to variability and trends of global gross primary productivity *Environmental Research Letters*, 12, 105003

Choudhury, B. (2000) Carbon-use efficiency and net primary productivity of terrestrial vegetation *Adv.Space.Res.* 26, 1105-1108

Chu, H., Baldocchi, D., Ranjeet, J., Wolf, S., Reichstein, M. (2017) Fluxes all the time? A primer on the temporal representativeness of FLUXNET *JGR Biogeosci.*, 122, 289-307

Ciais, P., Rayner, F., Chevalier, P., Bousquet, M., Logan, P., Peyline, P., Ramonet, M., (2010) Atmospheric inversions for estimating CO_2 fluxes: methods and perspectives *Clim.Change* 103, 69-92

Clark, D., Brown, S., Kicklighter, D., Chambers, J., Thomlinson, J., Ni, J., Holland, E. (2001), Net Primary Production in Tropical Forests, an Evaluation and Synthesis of Existing Field Data *Ecological Applications*, 11(2), 371-384

Cleveland, C., Taylor, P., Chadwick. K., Dahlin, K., Doughty, C., Malhi, Y., Smith, W., Sullivan, B., Wieder,W., Townsend, A., (2015) A comparison of plot-based, satellite and earth system model estimates of tropical forest net primary production *GBC*, 29, 626-644

Cox, P., Betts, R., Bunton, C., Essery, R., Rowntree, P., Smith, J. (1999) The impact of new land surface physics on the GCM simulation of climate and climate sensitivity *J.Climate Dynamics* 15, 183-203

Cramer, W., Kicklighter, D., Bondeau, A., Moore, B., Churkina, G., Nemry, B., Ruimy, A., Schloss, A., and the Participants of the Potsdam NPP Model Intercomparison (1999) Comparing global models of terrestrial net primary productivity (NPP): overview and key results *Global Change Biology*, 5, Supplement 1, 1-15

Dai, A., Qian, T., Trenberth, K. (2009) Changes in continental freshwater discharge from 1948 to 2004 *Journal of Climate*, 22, 2773-2792

De Kauwe, M.G.; Disney, M.I.; Quaife, T.; Lewis, P.; Williams, M. (2011) An assessment of the MODIS collection 5 leaf area index product for a region of mixed coniferous forest *Remote Sensing of Environment*, 115, 767-780

DeLucia, E., Drake, J., Thomas, R., Gonzalez-Meler, M., (2007) Forest carbon use efficiency: is respiration a constant fraction of gross primary production ? *Global Change Biology*, 13, 1157-1167

Elmendorf, S., Gregory H., Hollister, R. (2012) Plot-scale evidence of tundra vegetation change and links to recent summer warming *Nature Climate Change*, 2, 453-457

Field CB, Randerson, JT, Malmstrom CM. (1995) Global net primary production: Combining ecology and remote sensing. *Remote Sensing of Environment* 51: 74-88

Friend, A., Arneth, A., Kiang, N., Lomas, M., Ogee, J., Roedenbeck, C., Running, S., Santaren, J., Sitch, S., Viovy, N., Woodward, I., Zaehle, S., (2007) FLUXNET and modelling the global carbon cycle *Global Change Biology*, 13, 610-633

Fu, Z., Gerken, T., Bromley, G., Arajo, A., Bonal, D., Burban, B., Ficklin, D., Fuentes, J. D., Goulden, M., Hirano, T., Kosugi, Y., Liddell, M., Nicolini, G., Niu, S., Roupsard, O., Stefani, P., Mi, C., Tofte, Z., Xiao, J., Valentini, R.,Wolf, S., and Stoy, P. C., (2018) The surface-atmosphere exchange of carbon dioxide in tropical rainforests: Sensitivity to environmental drivers and flux measurement methodology *Agricultural and Forest Meteorology*, 263, 292-307

Gill, R., Kelly, R., Parton, W., Day, K., Jackson, R., Morgan, J., Scurlock, J., Tieszen, L, Castle, J., Ojima, D., Zhang, X. (2002) Using simple environmental variables to estimate belowground productivity in grasslands *Global Ecology & Biogeography*, 11, 79-86

Goldwijk, K., Beusen, A., van Drecht, G., de Vos, M., (2011) The HYDE 3.1 spatially explicit database of human-induced global land-use change over the past 12,000 years *Global Ecology and Biogeography*, 20, 73-86

Gurevitch, J., Scheiner, S., Fox, G., (2006), Chpt 17, The Ecology of Plants, *Ed. Sinauer Associates, Sunderland, USA*

Gurney, K. R., Law, R. M., Denning, A. S., Rayner, P. J., Baker, D., Bousquet, P., Bruhwiler, L., Chen, Y.-H., Ciais, P., Fan, S., Fung, I. Y., Gloor, M., Heimann, M., Higuchi, K., John, J., Maki, T., Maksyutov, S., Masarie, K., Peylin, P., Prather, M., Pak, B. C., Randerson, J., Sarmiento, J., Taguchi, S., Takahashi, T., and Yuen, C.-W. (2002) Towards robust regional estimates of CO2 sources and sinks using atmospheric transport models, *Nature*, 415, 626-630

Hargrove, W., Hoffman, F., Law, B., (2003) *EOS Transactions American Geophysical Union*, 84, 529-544

Hansen, M., Reed, B., (2000) A comparison of the IGBP DISCover and University of Maryland 1 km global land cover products *Int. J. Remote Sensing*, 21, 1365-1373

Haughton, N., Abramowitz, G., De Kauwe, M., Pitman, A. (2018) Does predictability of fluxes vary between FLUXNET sites? *Biogeosciences*, 15, 4495-4513

He, H., Zhang, L., Gao, Y., Ren, X., Zhang, L., Guirui, Y., Wang, S., (2015) Regional representativeness assessment and improvement of eddy flux observations in China *Science of the Total Environment*, 502, 688-698

Heinsch, F., Zhao, M., Running, S. (2006) Evaluation of remote sensing based terrestrial productivity from MODIS using regional tower eddy flux network observations *IEEE Transactions on Geoscience and Remote Sensing*, 44, 1908-1925

Hollinger, D., Richardson, A. (2005) Uncertainty in eddy covariance measurements and its application to physiological models *Tree Physiology*, 25, 873-885

Houghton, R., Skole, D., (1990) in The Earth as Transformed by Human Action by Turner, B., Clark, W., Kates, R., Richards, J., Mathews, J., Meyer, W. *Cambridge University Press*, Cambridge

Ito, A. (2011) A historical meta-analysis of global terrestrial net primary productivity: are estimates converging? *Global Change Biology*, 17, 3161-3175

Jasechko, S., Sharp, Z., Gibson, J., Birks, S., Yi, Y., Fawcett, P. (2013) Terrestrial water fluxes dominated by transpiration *Nature*, 496, 347-351

Joiner, J., Yoshida, Y., Zhang, Y., Duveiller, G., Jung, M., Lyapustin, A., Wang, Y., Tucker, C. (2018), Estimation of terrestrial global primary production (GPP) with satellite data-driven models and eddy covariance flux data *Remote Sens.*, 10, 1346

Jung, M., Reichstein, M., and Bondeau, A.: Towards global empirical upscaling of FLUXNET eddy covariance obser- vations: validation of a model tree ensemble approach using a biosphere model (2009) *Biogeosciences*, 6, 2001-2013

Kattge, J., Knorr, W., Raddatz, T., Wirth, C. (2009) Quantifying photosynthetic capacity and its relationship to leaf-Nitrogen content for global-scale terrestrial biosphere models *Global Change Biology*, 15, 976-991

Keeling, C., Chin, J., Whorf, T., (1996) Increased activity of northern vegetation inferred from atmospheric CO_2 measurements *Nature*, 382, 146-149

Keenan, T., Prentice, I. C., Canadell, J., Williams, C., Wang, H., Raupach, M., Collatz, G. (2016) Recent pause in the growth rate of atmospheric CO_2 due to enhanced terrestrial carbon uptake *Nature Communications*, 7, 13428

Knorr, W. and Heimann, M. (2001) Uncertainties in global terrestrial biosphere modeling, Part I: A comprehensive sensitivity analysis with a new photosynthesis and energy
Koffi, E., Rayner, P., Scholze, M., Beer, C., (2012) Atmospheric constraints on gross primary productivity and net ecosystem productivity: results from a carbon-cycle data assimilation system *Global Biogeochemical Cycles*, 26, GB1024

Kumar, J., Hoffman, F. M., Hargrove, W. W., and Collier, N. (2016), Understanding the representativeness of FLUXNET for upscaling carbon flux from eddy covariance measurements, *Earth Syst. Sci. Data Discuss*, 2016, 1-25, doi:10.5194/essd-2016-36

Lasslop, G., Reichstein, M., Papale, D., Richardson, A., Arneth, A., Barr, A., Stoy, P., Wohlfahrt, G., (2010) Separation of net ecosystem exchange into assimilation and respiration using a light response curve approach: critical issues and global evaluation *Global Change Biology*, 16, 187-208

Le Quéré, C., R. Moriarty, R. M. Andrew, J. G. Canadell, S. Sitch, J. I. Korsbakken, P. Friedlingstein, G. P. Peters, R. J. Andres, T. A. Boden, R. A. Houghton, J. I. House, R. F. Keeling, P. Tans, A. Arneth, D. C. E. Bakker, L. Barbero, L. Bopp, J. Chang, F. Chevallier, L. P. Chini, P. Ciais, M. Fader, R. A. Feely, T. Gkritzalis, I. Harris, J. Hauck, T. Ilyina, A. K. Jain, E. Kato, V. Kitidis, K. Klein Goldewijk, C. Koven, P. Landschuetzer, S. K. Lauvset, N. Lefevre, A. Lenton, I. D. Lima, N. Metzl, F. Millero, D. R. Munro, A. Murata, J. E. M. S. Nabel, S. Nakaoka, Y. Nojiri, K. OBrien, A. Olsen, T. Ono, F. F. Perez, B. Pfeil, D. Pierrot, B. Poulter, G. Rehder, C. Roedenbeck, S. Saito, U. Schuster, J. Schwinger, R. Seferian, T. Steinhoff, B. D. Stocker, A. J. Sutton, T. Takahashi, B. Tilbrook, I. T. van der Laan-Luijkx, G. R. van der Werf, S. van Heuven, D. Vandemark, N. Viovy, A. Wiltshire, S. Zaehle, N. Zeng (2015) Global Carbon Budget 2015. Earth Syst. Sci. Data 7, 349-396

Li, Z., Liu, Shuguang; Tan, Zhengxi; Bliss, Normann B.; Young, Claudia J.; West, Tristram O.; and Ogle, Stephen M., (2014) Comparing cropland net primary production estimates from inventory, a satellite-based model, and a process-based model in the Midwest of the United States *Ecological Modelling*, 277, 1-12

Liang, M., Mahata, S., Laskar, A., Thiemens, M., Newman, S., (2017) Oxygen isotope anomaly in tropospheric CO_2 and implications for CO_2 residence time in the atmosphere and gross primary productivity *Nature*, 7, 13180

Loveland, T.R., Reed, B.C., Brown, J.F., Ohlen, D.O., Zhu, Z., Yang, L. & Merchant, J.W. (2000) Development of a global land cover characteristics database and IGBP DISCover from 1 km AVHRR data. International Journal of Remote Sensing, 21, 1303-1330

Malhi, Y., Doughty, C., Galbraith, D., (2011) *Phil.Trans.R.Soc.B*, 366, 3225-3245

Malhi, Y., Grace, J. (2000) Tropical Forests and Atmospheric Carbon Dioxide *Trends in Ecology & Evolution*, 15(8):332-337

Medlyn, B., Robinson, A., Clement, R., McMurtie, E. (2005) On the validation of models of forest CO_2 exchange using eddy covariance data: some perils and pitfalls *Tree Physiology* 25, 839-857

Monteith, J.L. (1965) Evaporation and environment. *Symp. Soc. Exptl. Biol.* 19, 205-234.

Myneni, R., Keeling, C., Tucker, C., Asrar, G., Nemani, R., (1997) Increased plant growth in the northern high latitudes from 1981 to 1991 *Nature*, 386, 698-702

Nemani RR, Keeling CD, Hashimoto H, Jolly WM, Piper SC, Tucker CJ, Myneni RB, Running SW. (2003) Climate-driven increases in global terrestrial net primary production from 1982 to 1999. *Science*, 300, 1560-1563

Olson, R. J., J. M. O. Scurlock, S. D. Prince, D. L. Zheng, and K. R. Johnson (eds.). 2008. NPP Multi-Biome: NPP and Driver Data for Ecosystem Model-Data Intercomparison, R[evision]1. Data set. Available on-line [http://www.daac.ornl.gov] from the Oak Ridge National Laboratory Distributed Active Archive Center, Oak Ridge, Tennessee, U.S.A.

Papale, D., Black, T.A., Carvalhais, N., Cescatti, A., Chen, J., Jung, M., Kiely, G., Lasslop, G., Mahecha, M.D., Margolis, H., Merbold, L., Montagnani, L., Moors, E., Olesen, J.E., Reichstein, M., Tramontana, G., van Gorsel, E., Wohlfahrt, G., R'aduly, B., (2015), Effect of spatial sampling from Europeanflux towers for estimating carbon and waterfluxes with artificial neural networks, *J.Geophys.Res.Biogeosci.*,120, 1941-1957, doi:10.1002/2015JG002997

Prentice, I., Liang, X., Medlyn, B., Wang, Y.-P., (2015) Reliable, robust and realistic: the three R's of next-generation land-surface modelling *Atmos.Chem.Phys.*, 15, 5987-6005

Quaife, T., Quegan, S., Disney, M., Lewis, P., Lomas, M., Woodward, F. (2008) Impact of land cover uncertainties on estimates of biospheric carbon fluxes *Global Biogeochemical Cycles*, 22, GB4016

Reichstein M, Falge E, Baldocchi D.,Dario Papale,Marc Aubinet,Paul Berbigier,Christian Bernhofer,Nina Buchmann,Tagir Gilmanov,Andr Granier,Thomas Grünwald Katka Havránková,Hannu Ilvesniemi,Dalibor Janous,Alexander Knohl,Tuomas Laurila,Annalea Lohila,Denis Loustau,Giorgio Matteucci,Tilden Meyers,Franco

Miglietta,Jean-Marc Ourcival,Jukka Pumpanen,Serge Rambal,Eyal Rotenberg,Maria Sanz,John Tenhunen,Gnther Seufert,Francesco Vaccari,Timo Vesala,Dan Yakir ,Riccardo Valentini (2005) On the separation of net ecosystem exchange into assimilation and ecosystem respiration: review and improved algorithm. *Global Change Biology* ,11, 1424-1439.

Ryu, Y., Baldocchi, D., Kobayashi, H., van Inge, C., Lie, J. (2011) Integration of MODIS land and atmosphere products with a coupled-process model to estimate gross primary productivity and evapotranspiration from 1 km to global scales *Global Biogeochemical Cycles* 25(4), GB4017

Schimel, D., Pavlick, R., Fisher, J., Asner, G., Saatchi, S., Townsend, P., Miller, C., Frankenberg, C., Hibbard, K., Cox, P., (2015) Observing terrestrial ecosystems and the carbon cycle from space *Global Change Biology*, 21, 1762-1776

Sellers, P., Dickinson, R., Randall, D. (1997) Modeling the exchanges of energy, water and carbon between continents and the atmosphere *Science* 275, 502-509

Sheffield, J., G. Goteti, and E. Wood (2006), Development of a 50-year high-resolution global dataset of meteorological forcings for land surface modeling, *J. Clim.*, 19, 3088–3111.

Sheffield, J., Wood,E., Roderick, M. (2012) Little change in global drought over the past 60 years *Nature*, 491, 435-438

Still, C. J., J. A. Berry, G. J. Collatz, and R. S. DeFries (2003), Global distribution of C_3 and C_4 vegetation: Carbon cycle implications, *Global Biogeochem. Cycles*, 17(1), 1006, doi:10.1029/2001GB001807

Stoy, P., Richardson, A., Baldocchi, D., G.G.Katul, J.Stanovick, M.D.Mahecha, M.Reichstein, M.Detto, B.E.Law, G.Wohlfahrt, N.Arriga, J.Campos, J.H.McCaughey, L.Montagnani, K.T.Paw U, S.Sevanto, and M.Williams (2009) Biosphere-atmosphere exchange of CO_2 in relation to climate: a cross-biome analysis across multiple timescales *Biogeosciences*, 6, 2297-2312

Strahler, A., Strahler, A., (2013) Modern Physical Geography, 6th Edition, Chapter 7, John Wiley & Sons, New York

Sulkava, M., Luyssaert, S., Zaehle, S., Papale, D. (2011) Assessing and improving the representativenss of monitoring networks: the European flux tower network example *JGR*, 116, G00J04

Sundareshwar PV, Murtugudde R, Srinivasan G, Singh S, Ramesh KJ,Ramesh R, Verma SB, Agarwal SB, Baldocchi D, Baru CK, Baruah KK, Chowdhury GR, Dadhwal VK, Dutt CBS, Fuentes J, Gupta PK, Hargrove WW, Howard M, Jha CS, Lal S, Michener WK, Mitra AP, Morris JT, Myneni RR, Naja M, Nemani R, Purvaja R, Raha SKSVS, Sharma M, Subramaniam A, Sukumar R, Twilley RR, Zimmerman PR. (2007). Environmental monitoring network for India. *Science*, 316, 204-205

Topping J. (1975) Errors of observation and their treatment, Chapman & Hall, London.

van Iersel, M. (2003) Carbon use efficiency depends on growth respiration, maintenance respiration, and relative growth rate. A case study with lettuce *Plant, Cell and Environment*, 26 (9), 1441-1449.

Waring RH, Landsberg JJ, Williams M (1998) Net primary production of forests: a constant fraction of gross primary production? *Tree Physiology*,18, 129

Waring, R., Running, S., (1998) Forest Ecosystems: Analysis at Multiple Scales 370pp, Academic Press, San Diego, California

Welp, L., Keeling, R., Meijer, H., Bollenbacher, A., Piper, S., Yoshimura, K., Francey, R., Allison, C., Wahlen, M. Interannual variability in the oxygen isotopes of atmospheric CO_2 driven by El Nino *Nature*, 477, 579-582

Whittaker R.H. (1975) Communities and ecosystems (2nd edn). Macmillan, New York, USA.

Wilson, K., Goldstein, A., Falge, E., Aubinet M., Baldocchi D., Berbigier P., Bernhofer C., Ceulemans R., Dolman H., Field C., Grelle A., Ibrom A., Law B.E., Kowalski A., Meyers T., Moncrieff J., Monson R., Oechel W., Tenhunen J., Valentini R., Verma S. (2002) Energy balance closure at FLUXNET sites *Agricultural & Forest Meteorology*, 113, 223-243

Xiao, J., Chen, J., Davis, K., Reichstein, M. (2012), Advances in upscaling of eddy covariance measurements of carbon and water fluxes *J.Geophysical Res.*, 117, G00J01

Yan, K., Park., T., Yan, G., Liu, A., Yang, B., Chen, C., Nemani, R., Knyazikhin, Y., Myneni, R. (2016) Evaluation of MODIS LAI/FPAR Product Collection 6. Part 2: validation and intercomparison *Remote Sensing*, 8, 460-485

Yang, W., Bin Tan, Dong Huang, Miina Rautiainen, Nikolay V. Shabanov, Y. Wang, Jeffrey L. Privette, Karl Fred Huemmrich, Rasmus Fensholt, Inge Sandholt, M. Weiss, Douglas E. Ahl, Stith T. Gower, Ramakrishna R. Nemani, Yuri Knyazikhin, and Ranga B. Myneni (2006a). MODIS Leaf Area Index Products: From Validation to Algorithm Improvement *IEEE Trans. Geosci. Remote Sens.*, 44: 1885-1898

Yang, W, Shabanov, NV, Huang, D, Wang, W, Dickinson, RE, Nemani, RR, Knyazikhin, Y, Myneni, RB (2006b). Analysis of leaf area index products from combination of MODIS Terra and Aqua data. *Remote Sensing of Environment*, 104(3), 297-312

Yang, F., Zhu, X-A., Kazuhito, I., White, M., Hashimoto, H., Nemani, R., (2008) Assessing the representativeness of the AmeriFlux network using MODIS and GOES data *Journal of Geographical Research*, 113, G04036

Yebra, M., Van Dijk, A., Leuning, R., Guerschman, J., (2015) Global vegetation gross primary production estimation using satellite-derived light-use efficiency and canopy conductance *Remote Sens.Environ.*, 163, 206-216

Yuan W., Liu, S., Yu, G., Bonnefond, J., Chen, J., Davis,K., Desai, A., Goldstein, A., Gianelle, D., Rossi, F., Suyker, A., Verma, S. (2010) Global estimates of evapotranspiration and gross primary production based on MODIS and global meteorology data *Remote Sens.Environ.*, 114, 1416-1431

Zaehle, S., Sitch, S., Smith, B., and Hatterman, F. (2005) Effects of parameter uncertainties on the modeling of terrestrial biosphere dynamics. Global Biogeochem. Cycles, 19, GB3020

Zaks, D., Ramankutty, N., Barford, C., Foley, J. (2007) From Miami to Madison: investigating the relationship between climate and terrestrial net primary production *Global Biogeochem. Cycles*, 21, GB3004

Zhao, M., Heinsch, F., Nemani, R., Running, S., (2005) Improvements of the MODIS terrestrial gross and net primary production global data set *Remote Sensing of Environment*, 95, 164-176

Zhao, M., Running, S., (2009) Drought-induced reduction in global terrestrial net primary production from 2000 through 2009 *Science*, 329, 940-943

Zhang, Y., Xu, M., Chen, H., Adams, J. (2009) Global pattern of NPP to GPP ratio derived from MODIS data; effects of ecosystem type, geographical location and climate *Global Ecology and Biogeography*, 18, 280-290

Zhang, Y., Conghe, S., Band., L., Sun, G., Li, J. (2017a) Reanalysis of global terrestrial vegetation trends from MODIS products: browning or greening? *Remote Sensing of Environment*, 191, 145-155

Zhang, Y., Xiao, X., Wu, X., Zhou, S., Zhang, G., Qin, Y., Dong, J. (2017b) A global moderate resolution dataset of gross primary production of vegetation for 2000-2016 *Sci.Data* 4:170165

Zhang, Y., Kong, D., Gan, R., Chiew, F., McVicar, T., Zhang, Q., Yang, Y., (2019) Coupled estimation of 500 m and 8-day resolution global evapotranspiration and gross primary production in 2002-2017 *Remote Sensing of Environment*, 222, 165-182

Table 1: An alphabetical list of acronyms, abbreviations and quantities used frequently in the main text. Units are given where appropriate.

	Definition
CUE	Carbon-Use Efficiency
EMDI	Ecosystem Model-Data Intercomparison
FLUXNET2015	Flux Network (2015 release)
GPP	Gross Primary Productivity (Gt yr^{-1} or kg m^{-2} yr^{-1})
LAI	Leaf Area Index (m^2 m^{-2})
$\overline{LAI}_{max}$	mean maximum seasonal LAI (m^2 m^{-2})
LUE	Light-Use Efficiency
MAP	Mean Annual Precipitation (mm yr^{-1})
MAT	Mean Annual Temperature (°C)
MASW	Mean Annual ShortWave radiation (W m^{-2})
MODIS	Moderate Resolution Imaging Spectroradiometer
NPP	Net Primary Productivity (Gt yr^{-1} or kg m^{-2} yr^{-1})
PFT	Plant Functional Type

Table 2: The numerical representativeness of each plant functional type (PFT) within the carbon-monitoring networks (FLUXNET2015 and EMDI) compared to corresponding global 0.5° land-points. The percentage of sites (or vegetated global area) within each vegetation class is indicated and the number of sites, where applicable, is shown in parentheses. LaThuile is an extended FLUXNET network (Stoy et al 2009) for which a harmonised dataset of site GPP might be expected to become available in the future. For the LaThuile network, we aggregate grasses and crops since data are not always available to reliably distinguish between C3 and C4. The bottom row shows the global number of sites for each network. The second left-most column indicates the PFT abbreviation adopted in subsequent tables and figures.

PFT	PFT abbreviation	EMDI %(n)	FLUXNET2015 %(n)	LaThuile %(n)	Global %
Non-tropical Broadleaf Forest	BL	18.5(51)	16.9(26)	24.0(106)	1.9
Non-mediterranean Needleleaf Forest	NL	21.0(58)	21.4(33)	17.9(79)	26.8
C3 crop	Cr3	4.0(11)	10.4(16)	12.2(54)	10.6
C4 crop	Cr4	1.1(3)	3.2(5)		1.0
Tundra Shrub	Tu	4.3(12)	1.3(2)	0.7(3)	8.6
Mixed Forest	MX	3.6(10)	5.2(8)	4.1(18)	4.5
Tropical Broadleaf Forest	TBL	8.0(22)	3.2(5)	5.9(26)	9.1
C3 grass	C3	5.4(15)	16.9(26)	19.3(85)	22.9
C4 grass	C4	14.1(39)	2.6(4)		6.9
Non-tundra Shrub	SH	4.7(13)	7.1(11)	6.3(28)	1.7
Savanna	SAV	1.8(5)	8.4(13)	5.9(26)	5.4
Mediterranean Needleleaf Forest	MNL	13.4(37)	3.2(5)	3.6(16)	0.7
Global		(276)	(154)	(441)	

Table 3: Previous estimates of global Net Primary Productivity (NPP) and Gross Primary Productivity (GPP) compared to upscaled estimates from the current study (in bold). Summary estimates for NPP are taken from the comprehensive review and compilation of Ito (2011), aggregating the mean averages of various methodological subgroups. BGC and DGVM are biogeochemical and dynamic global vegetations models, respectively. WUE is water-use efficiency. LUE and PEM are light-use efficiency and productivity-efficiency models. Indicative references for global GPP, which has far fewer estimates than NPP, are given in the far right column (see also the partial review and technique intercomparison of Anav et al (2015) and Zhang et al (2019)).

Technique	Global NPP		Global GPP		
	Range [Gt yr^{-1}]	Subgroup	Range [Gt yr^{-1}]	Subgroup	References
Empirical Scaling	46-54	inventory, empirical	120-130	inventory, statistical	Beer et al (2010); Zhang et al (2017b); Bodesheim et al (2018)
Process-based Modelling	56-61	BGC, DGVM	120-170	BGC, DGVM	Kattge et al (2009); Chen et al (2017); Ryu et al (2011); Alton (2013); Anav et al (2015)
LUE Models	49	LUE, PEMs	105-140	LUE, PEMs	Yuan et al (2010); Zhang et al (2009); Yebra et al (2015); Zhang et al (2017b); Joiner et al (2018)
WUE Approach	–	–	125-130	–	Beer et al (2010); Jasechko et al (2013)
Oxygen isotopes	–	–	120-175	–	Welp et al (2011); Liang et al (2017)
Atmospheric CO_2 Modelling	–	–	125-165	–	Koffi et al (2012)
Weighted Upscaling	**66±4**	–	**131±8**	–	this study

Table 4: The Net Primary Productivity (NPP) and Gross Primary Productivity (GPP) per Plant Functional Type (PFT) and as a global sum (last row). PFTs are ranked, with greatest contribution to global GPP at the top, and are abbreviated according to Tab. 2. Estimates for NPP and GPP are given both in Gt yr^{-1} and as a percentage of the global total. Uncertainties in Gt yr^{-1} are derived from the bootstrap error analysis. The global area occupied by each PFT is given in millions of km^2.

PFT	Area	NPP		GPP	
(-)	(mi.km^2)	(Gt yr^{-1})	(%)	(Gt yr^{-1})	(%)
TBL	13.8	14.1±1.0	22	37.8±6.0	29
C3	27.8	10.1±1.8	16	23.5±2.9	18
NL	19.9	8.5±0.7	13	22.6±1.9	17
Cr3	12.6	17.1±2.3	26	15.4±1.4	12
SAV	8.0	5.0±2.0	8	8.9±1.1	7
MX	5.1	2.8±0.3	5	8.5±1.0	6
C4	9.8	4.2±0.6	7	5.6±2.0	4
BL	2.1	1.3±0.1	2	3.5±0.1	3
Tu	5.6	0.5±0.1	1	1.6±0.4	1
SH	2.4	0.3±0.1	1	1.2±0.4	1
Cr4	1.4	1.2±0.2	2	1.1±0.1	1
MNL	0.9	0.4±0.1	1	1.1±0.3	1
global	109	66±4	100	131±8	100

Table 5: The climate distribution for global 0.5° cells, organised according to plant functional type (PFT), compared to sites classified with the same vegetation in the EMDI and FLUXNET2015 networks. MAP, MAT, MASW and $\overline{LAI}_{max}$ denote, respectively, Mean Annual Precipitation, Mean Annual Temperature, Mean Annual Shortwave radiation and mean maximum seasonal LAI. In each case we show the mean plus or minus the standard deviation. Values highlighted in bold indicate site means which lie more than two (global) standard deviations from the corresponding global mean. In the left-most column, the PFT is abbreviated according to Tab. 2. Sample sizes for EMDI and FLUXNET2015 are also given in Tab. 2.

PFT	Global				EMDI				FLUXNET2015			
	MAP [mm yr^{-1}]	MAT [°C]	MASW [W m^{-2}]	$\overline{LAI}_{max}$ [m^{2}m^{-2}]	MAP [mm yr^{-1}]	MAT [°C]	MASW [W m^{-2}]	$\overline{LAI}_{max}$ [m^{2}m^{-2}]	MAP [mm yr^{-1}]	MAT [°C]	MASW [W m^{-2}]	$\overline{LAI}_{max}$ [m^{2}m^{-2}]
BL	1130±500	12.6±4.1	160±30	3.3±1.1	990±460	12.6±6.9	150±40	3.7±1.2	830±320	11.5±4.0	160±20	3.9±1.5
NL	510±270	-3.9±5.4	110±20	2.3±1.0	890±500	5.4±4.5	140±30	3.5±1.1	710±390	4.3±4.9	140±30	3.2±1.1
Cr3	830±520	14.8±7.7	170±40	2.4±1.2	840±820	14.0±7.7	180±30	2.3±1.2	750±390	11.4±3.4	160±40	2.5±0.7
Cr4	1040±520	24.1±5.3	210±20	2.5±1.3	1430±950	20.0±9.4	190±30	2.2±1.1	720±180	**10.8±2.4**	180±30	2.5±0.5
Tu	290±210	-10.7±5.0	100±40	0.7±0.5	**810±580**	-0.7±5.7	120±30	**1.9±1.4**	170±10	-6.6±2.6	90±20	0.6±0.1
MX	1060±460	11.2±6.0	160±40	3.5±1.1	990±390	11.6±3.2	180±20	3.9±1.0	820±360	9.4±5.1	150±40	4.1±1.2
TBL	2260±750	25.9±1.7	200±10	5.6±1.2	2200±780	25.8±1.9	210±20	5.7±1.2	1750±850	23.2±2.1	190±30	5.5±1.7
C3	530±530	13.5±8.6	190±40	1.5±1.4	540±270	7.8±4.6	160±30	1.7±0.9	690±340	8.7±6.7	170±40	2.4±1.4
C4	610±410	24.2±4.3	230±20	1.5±1.1	820±390	21.6±5.4	210±20	2.2±1.2	690±420	21.9±3.9	250±10	1.6±1.1
SH	520±190	21.6±5.3	230±20	1.3±0.9	380±160	13.8±6.0	200±20	1.1±0.8	460±260	**7.8±10.8**	**180±50**	2.0±1.3
SAV	1250±470	25.4±2.3	220±10	3.4±1.2	600±310	27.4±1.2	220±10	1.7±1.0	780±510	23.3±4.2	230±20	1.7±0.8
MNL	550±210	1.7±2.7	210±20	1.0±0.8	**1240±630**	**13.3±4.5**	**170±20**	**3.4±1.3**	**1010±400**	**15.1±7.5**	200±40	**2.9±1.5**

Figure Captions:

Fig.1: Global Plant Functional Types (PFTs) based on Goldwijk et al (2011) with modification according to the distribution of C_4 vegetation (Still et al 2003). Grid-squares are at 0.5° resolution. PFTs are abbreviated according to Tab. 2. Land without vegetation is black.

Fig.2: Climate zones covered by the carbon-monitoring sites compared to global vegetated 0.5° landpoints (represented by dots). Climate is expressed as Mean Annual Temperature versus Mean Annual Precipitation. The delineated climate-biomes follow Whittaker (1975), namely: tundra (Tu), boreal forest (BF), temperate grassland (TeG), woody shrubland (WoSh), temperate deciduous forest (TeDF), temperate rain forest (TeRF), tropical deciduous forest (TrDF), tropical rain forest (TrRF), savanna (Sa) and desert (De).

Fig.3: Density of carbon-monitoring sites within temperature-precipitation space *versus* global 0.5° vegetated cells. Panel (a) combines all sites whereas panel (b) presents for individual carbon-monitoring networks. Density is recorded as number of locations (or global grid cells) per 500 mm yr^{-1} in mean annual precipitation and per 10°C in mean annual temperature. In panel (b) the vertical right axis has been scaled to allow a comparison between EMDI and FLUXNET2015. In panel (a), we annotate 2σ outliers from the linear fit.

Fig.4: The mean amplitude of seasonal Leaf Area Index (LAI) *versus* the mean maximum seasonal LAI ($\overline{LAI}_{max}$) for the carbon-monitoring networks, compared to global vegetated 0.5° cells (represented by dots). Amplitude is defined as the difference between the maximum and minimum LAI over the course of the year at the MODIS 8 day timestep. For both sites and global cells, the plotted amplitudes and maxima are averages over the period 2002-2008 (incl.). Displacement from the line y=x towards the bottom-right of the plot indicates a more evergreen habit.

Fig.5: The mean of w_{cell} averaged across all global 0.5° cells within the same PFT (w_{pft}) for FLUXNET2015 (vertical axis) and EMDI (horizontal axis). The quantity w_{cell} is defined in Eq. 2 using the inverse euclidian distance in climate-canopy space between global cells and relevant (same-PFT) carbon-monitoring sites. High values of w_{pft} ($\gtrsim$1) suggest that the network (FLUXNET2015 for GPP and EMDI for NPP) represents well the vegetation type ("good rep."). Poorly represented PFTs are towards the bottom-left ("poor rep."). PFTs are labelled according to Tab. 2.

Fig.6: Mean annual temperature *versus* latitude for 0.5° global cells (small dots) compared to sites of the same vegetation type within FLUXNET2015 and EMDI (large coloured markers). Panels (a) and (b) show, respectively, non-tundra shrub and non-mediterranean needleleaf forest. Note that both axes change their range between panels (a) and (b). For non-mediterranean needleleaf forest, there is a very small proportion of global cells (<1%) at latitudes $\simeq$ -50° which is not shown.

Fig.7: The modified mean inverse euclidian distance (w_{cell}) calculated for 0.5° global cells, with respect to FLUXNET2015, using Eq. 2. High values indicate good representativeness of the climate-canopy space by FLUXNET2015 sites of the same PFT as the cell. Non-vegetated areas are black. Crosses denote FLUXNET2015 locations.

Fig.8: The modified mean inverse euclidian distance (w_{cell}) calculated for 0.5° global cells, with respect to EMDI, using Eq. 2. High values indicate good representativeness of the climate-canopy space by EMDI sites of the same PFT as the cell. Non-vegetated areas are black. Crosses denote EMDI locations.

Fig.9: The ranges of Net Primary Productivity (NPP) and Gross Primary Productivity (GPP) for EMDI and FLUXNET2015 sites, respectively, expressed in kg m^{-2} yr^{-1}. Range is defined as mean-SD to mean+SD,

where SD is the standard deviation. Sites are grouped by PFT which is abbreviated according to Tab. 2. The filled circle is the mean GPP of each PFT multiplied by a reference Carbon-Use Efficiency (CUE=NPP/GPP) of 0.45.

Fig.10: Estimates of Net Primary Productivity (NPP; upper panel) and Gross Primary Productivity (GPP; lower panel) for PFTs which are well represented in terms of the original sample size (abbreviated according to Tab. 2). To compare different vegetation types, primary productivity is expressed per unit area (kg m^{-2} yr^{-1}) by averaging over all global grid cells of the corresponding PFT. The sample size used in the weighted global calculation of GPP (FLUXNET2015 sites) or NPP (EMDI sites) is decreased systematically from approximately the maximum number of available sites to a minimum of 3. Sample selection is based on a bootstrap method without replacement. Markers represent the mean across the bootstrap samples. Errorbars represent the standard deviation from the mean and reveal the uncertainty in GPP and NPP owing to limited sampling. For clarity, markers have been slightly offset from one another horizontally.

Fig.11: The GPP ratio versus NPP ratio for global vegetated 0.5° landpoints, shown separately for each PFT and labelled according to Tab. 2. The ratio equals the primary productivity simulated within the interpolated climate-canopy space, by the land-surface model JULES-SF, divided by the primary productivity simulated for the global climate-canopy space. Interpolated space depends on the distribution of carbon-monitoring sites for FLUXNET2015 and EMDI (§4.2). Similarity between the interpolated and global space should yield a ratio close to unity (dot-dash line). The dashed line (y=x) represents similar biases for NPP and GPP.

Figure 1: Global Plant Functional Types (PFTs) based on Goldwijk et al (2011) with modification according to the distribution of C_4 vegetation (Still et al 2003). Grid-squares are at 0.5° resolution. PFTs are abbreviated according to Tab. 2. Land without vegetation is black.

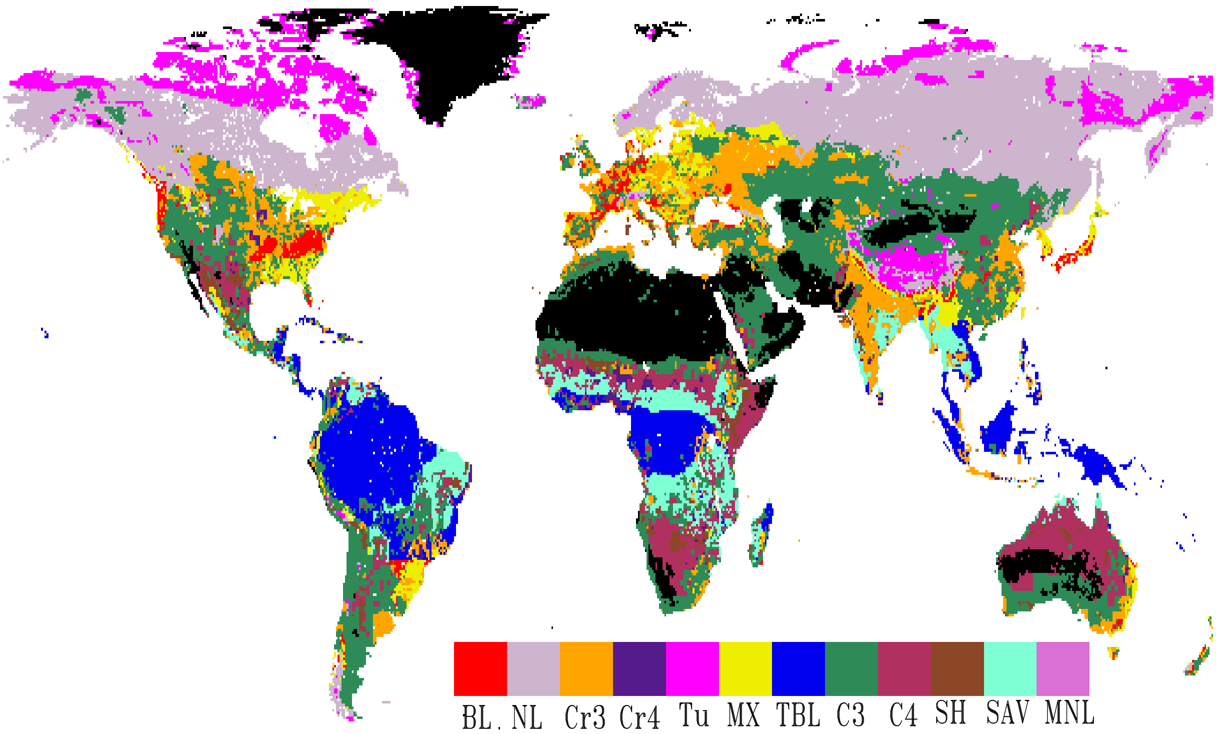

Figure 2: Climate zones covered by the carbon-monitoring sites compared to global vegetated 0.5° land-points (represented by dots). Climate is expressed as Mean Annual Temperature versus Mean Annual Precipitation. The delineated climate-biomes follow Whittaker (1975), namely: tundra (Tu), boreal forest (BF), temperate grassland (TeG), woody shrubland (WoSh), temperate deciduous forest (TeDF), temperate rain forest (TeRF), tropical deciduous forest (TrDF), tropical rain forest (TrRF), savanna (Sa) and desert (De).

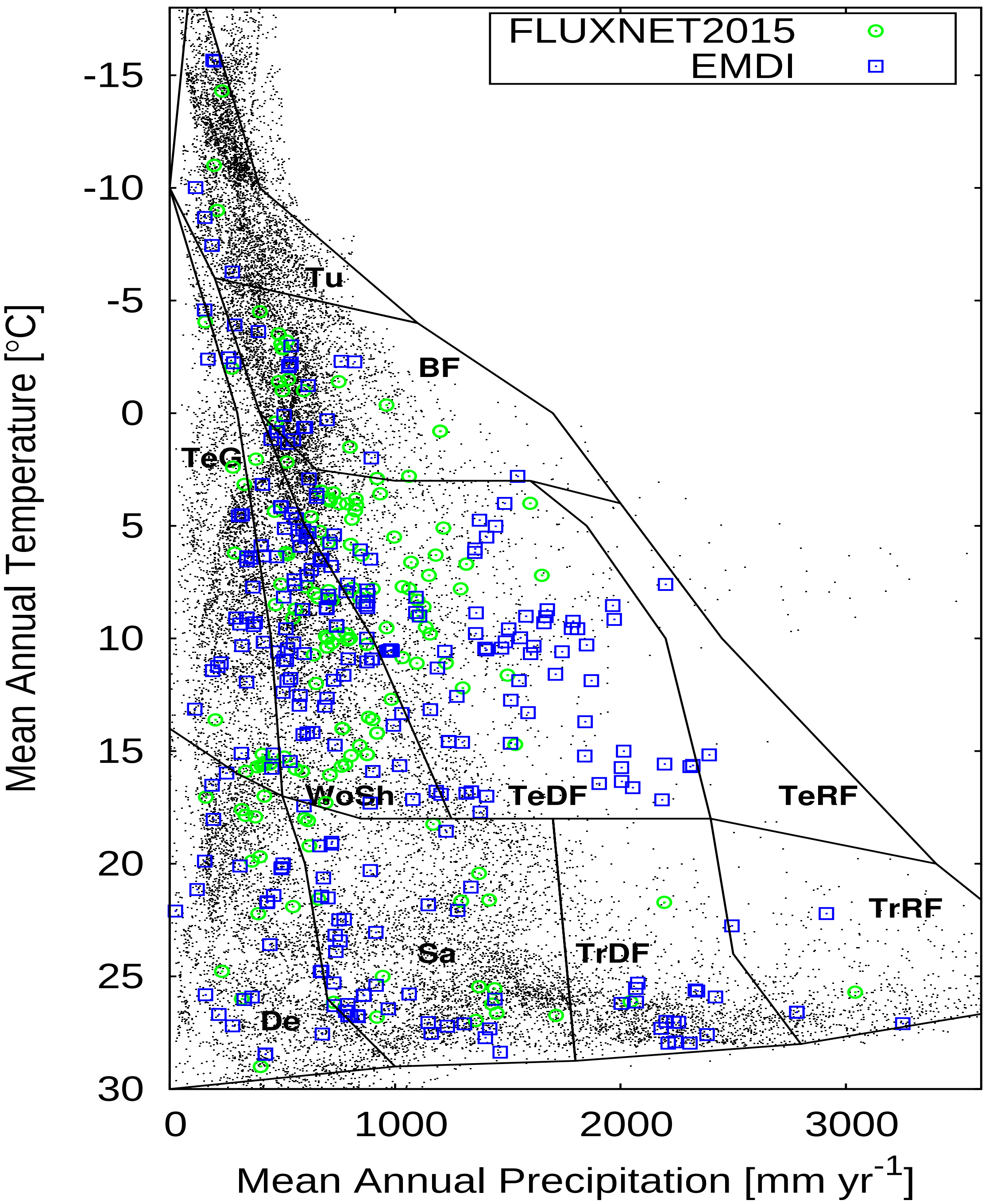

Figure 3: Density of carbon-monitoring sites within temperature-precipitation space *versus* global 0.5° vegetated cells. Panel (a) combines all sites whereas panel (b) presents for individual carbon-monitoring networks. Density is recorded as number of locations (or global grid cells) per 500 mm yr^{-1} in mean annual precipitation and per 10°C in mean annual temperature. In panel (b) the vertical right axis has been scaled to allow a comparison between EMDI and FLUXNET2015. In panel (a), we annotate 2σ outliers from the linear fit.

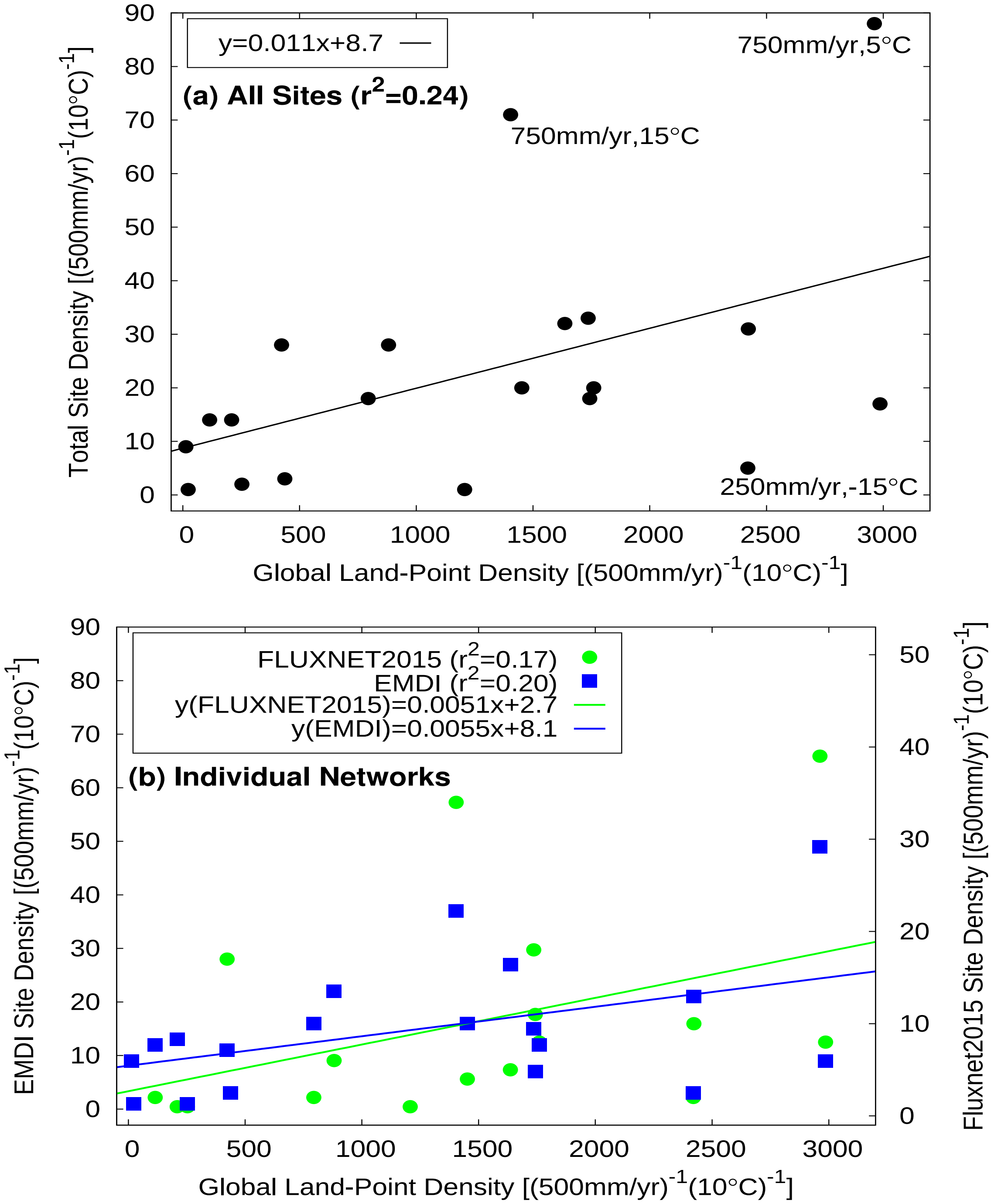

Figure 4: The mean amplitude of seasonal Leaf Area Index (LAI) *versus* the mean maximum seasonal LAI ($\overline{LAI}_{max}$) for the carbon-monitoring networks, compared to global vegetated 0.5° cells (represented by dots). Amplitude is defined as the difference between the maximum and minimum LAI over the course of the year at the MODIS 8 day timestep. For both sites and global cells, the plotted amplitudes and maxima are averages over the period 2002-2008 (incl.). Displacement from the line y=x towards the bottom-right of the plot indicates a more evergreen habit.

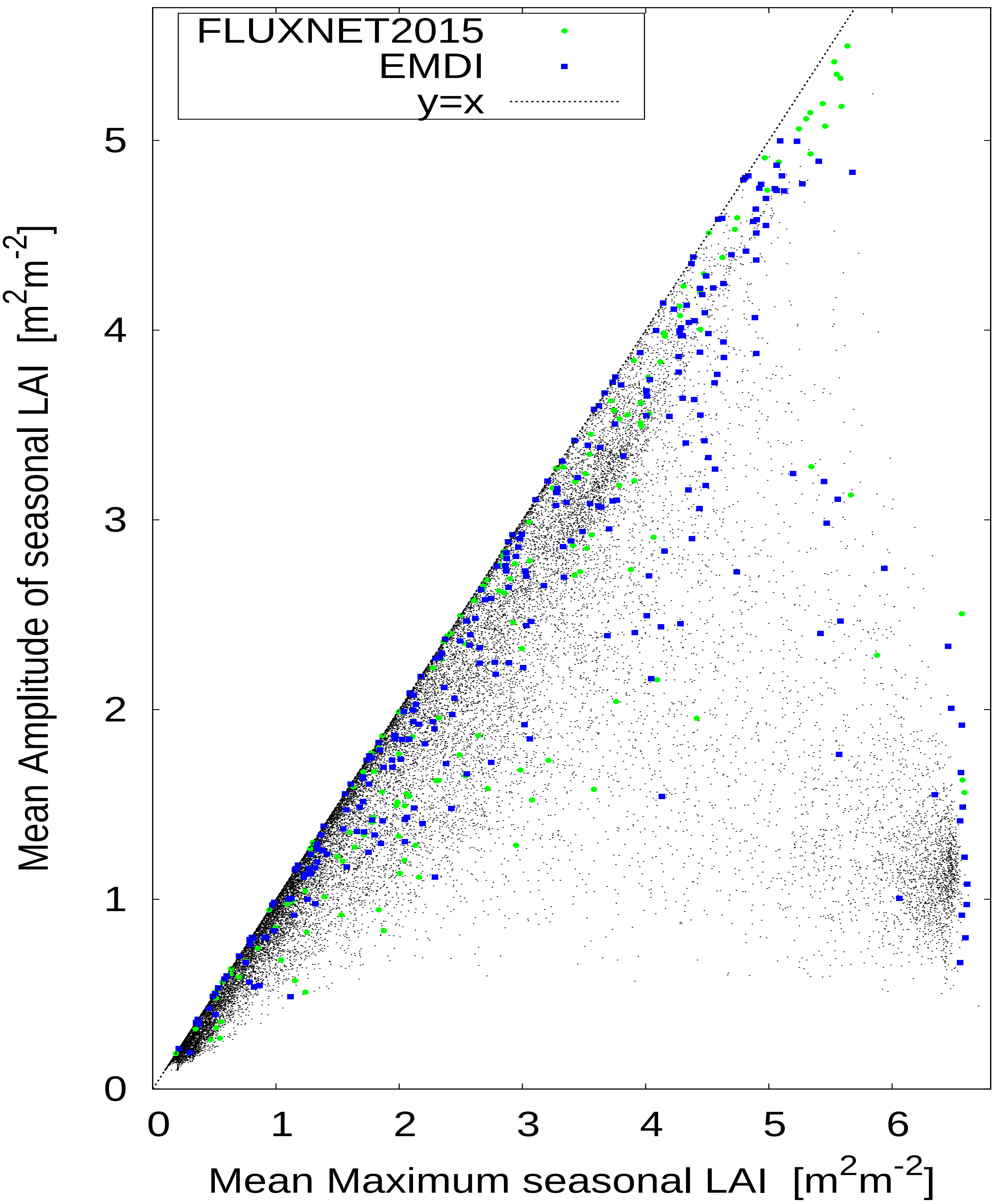

Figure 5: The mean of w_{cell} averaged across all global 0.5° cells within the same PFT (w_{pft}) for FLUXNET2015 (vertical axis) and EMDI (horizontal axis). The quantity w_{cell} is defined in Eq. 2 using the inverse euclidian distance in climate-canopy space between global cells and relevant (same-PFT) carbon-monitoring sites. High values of w_{pft} ($\gtrsim$1) suggest that the network (FLUXNET2015 for GPP and EMDI for NPP) represents well the vegetation type ("good rep."). Poorly represented PFTs are towards the bottom-left ("poor rep."). PFTs are labelled according to Tab. 2.

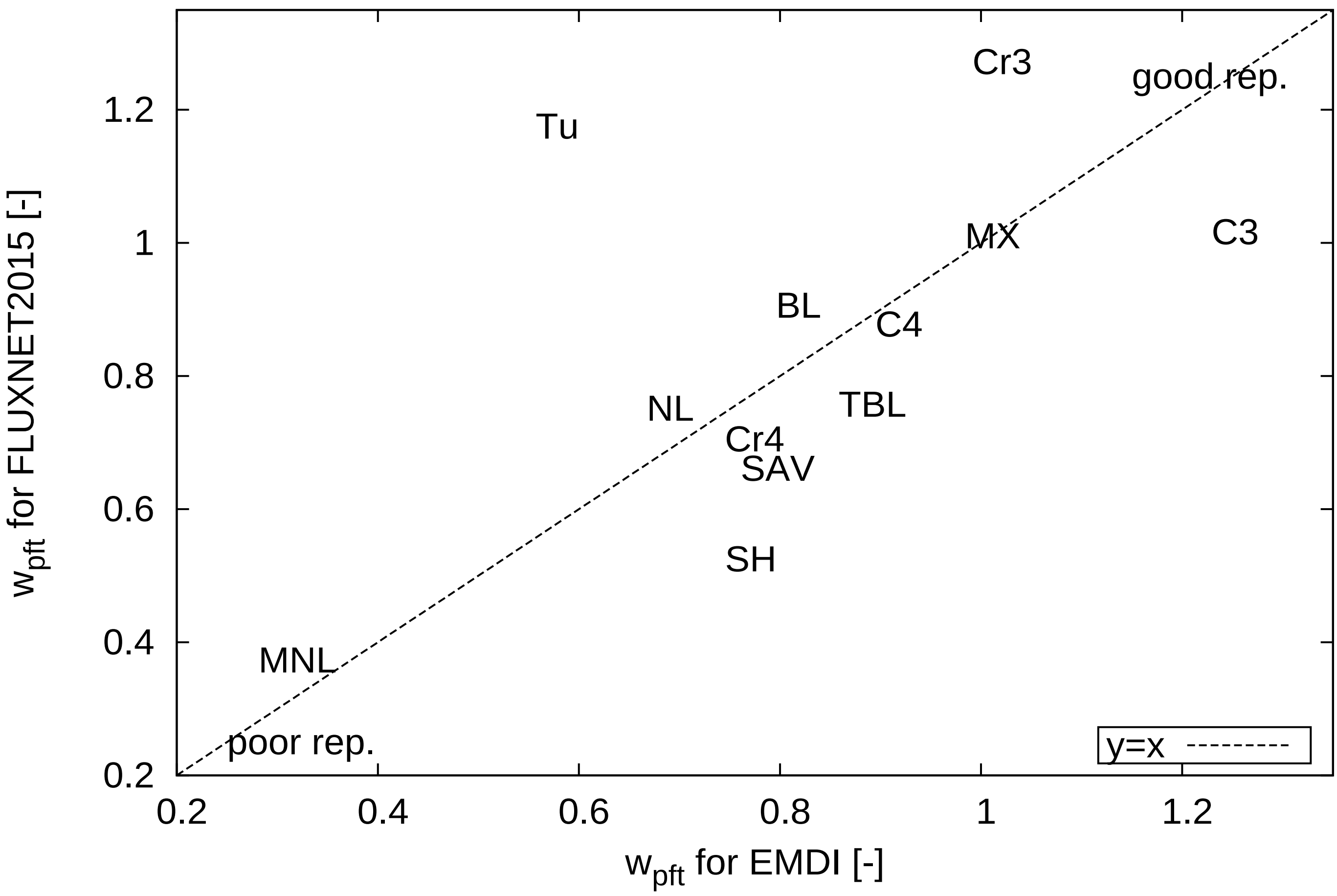

Figure 6: Mean annual temperature *versus* latitude for 0.5° global cells (small dots) compared to sites of the same vegetation type within FLUXNET2015 and EMDI (large coloured markers). Panels (a) and (b) show, respectively, non-tundra shrub and non-mediterranean needleleaf forest. Note that both axes change their range between panels (a) and (b). For non-mediterranean needleleaf forest, there is a very small proportion of global cells (<1%) at latitudes ≃ -50° which is not shown.

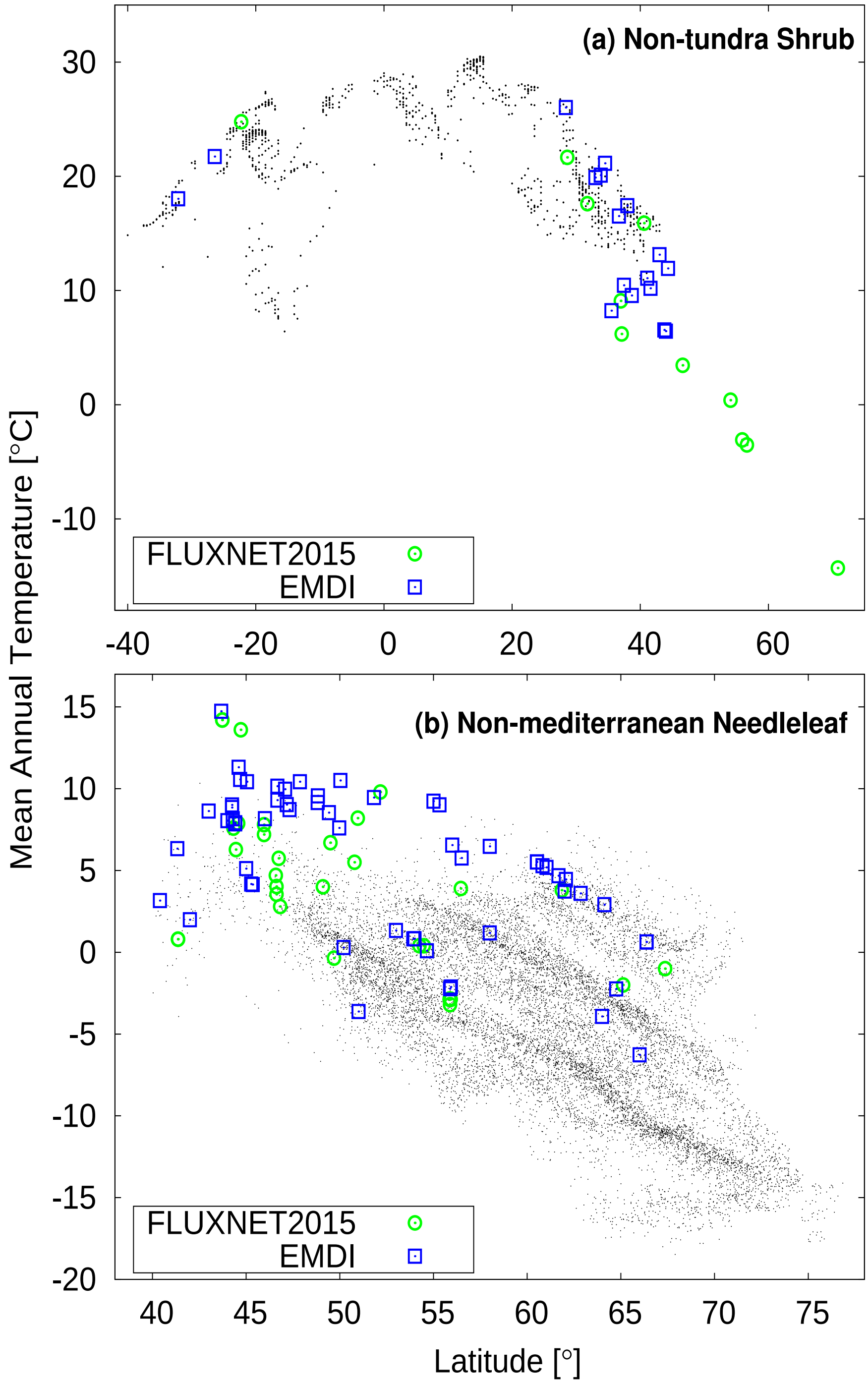

Figure 7: The modified mean inverse euclidian distance (w_{cell}) calculated for 0.5° global cells, with respect to FLUXNET2015, using Eq. 2. High values indicate good representativeness of the climate-canopy space by FLUXNET2015 sites of the same PFT as the cell. Non-vegetated areas are black. Crosses denote FLUXNET2015 locations.

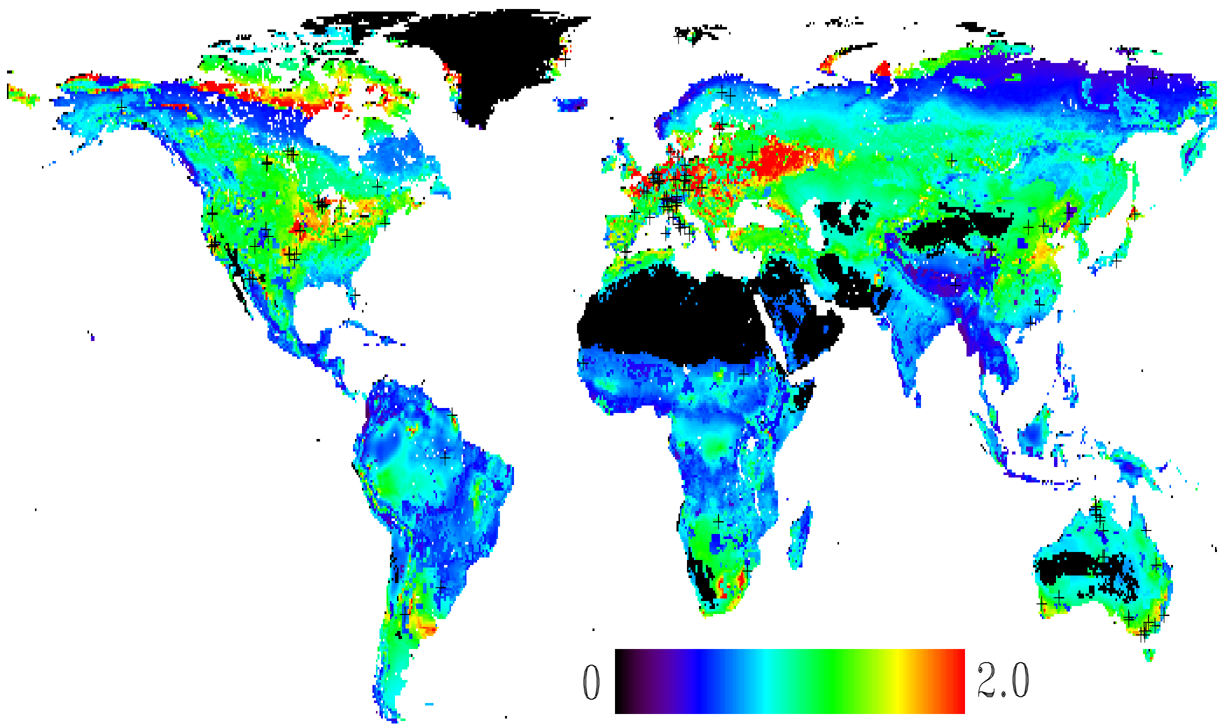

Figure 8: The modified mean inverse euclidian distance (w_{cell}) calculated for 0.5° global cells, with respect to EMDI, using Eq. 2. High values indicate good representativeness of the climate-canopy space by EMDI sites of the same PFT as the cell. Non-vegetated areas are black. Crosses denote EMDI locations.

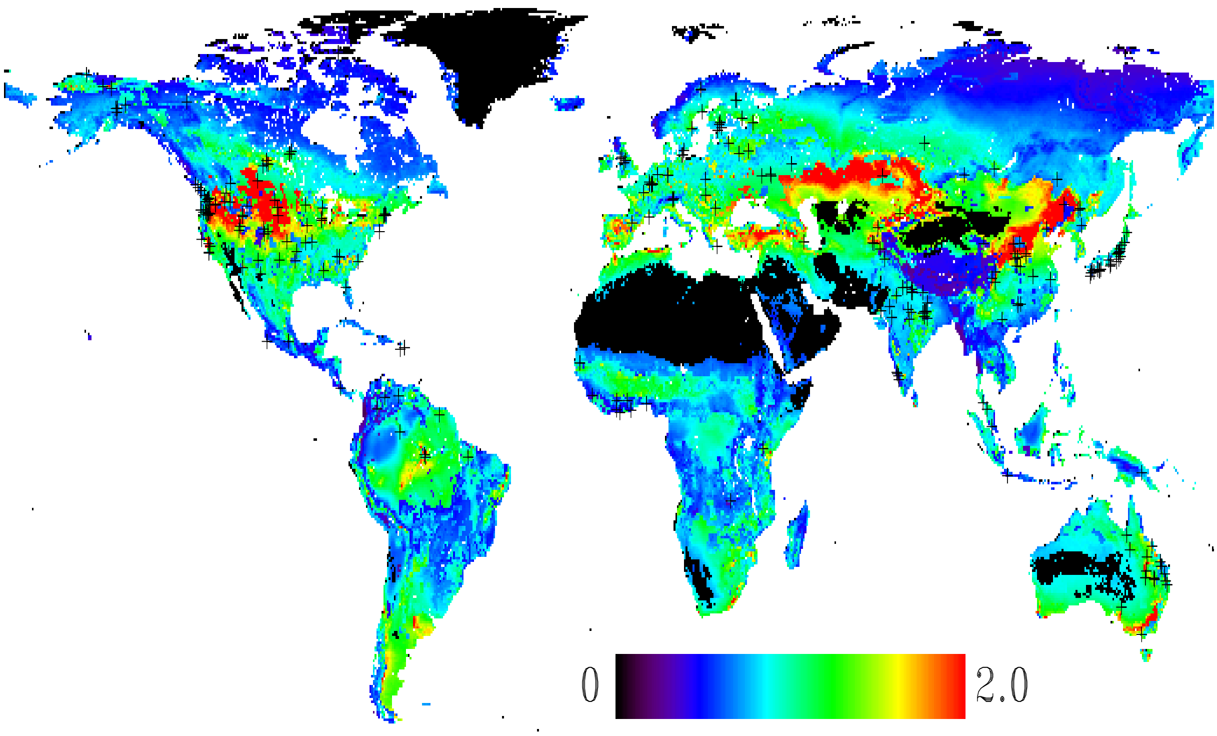

Figure 9: The ranges of Net Primary Productivity (NPP) and Gross Primary Productivity (GPP) for EMDI and FLUXNET2015 sites, respectively, expressed in kg m^{-2} yr^{-1}. Range is defined as mean-SD to mean+SD, where SD is the standard deviation. Sites are grouped by PFT which is abbreviated according to Tab. 2. The filled circle is the mean GPP of each PFT multiplied by a reference Carbon-Use Efficiency (CUE=NPP/GPP) of 0.45.

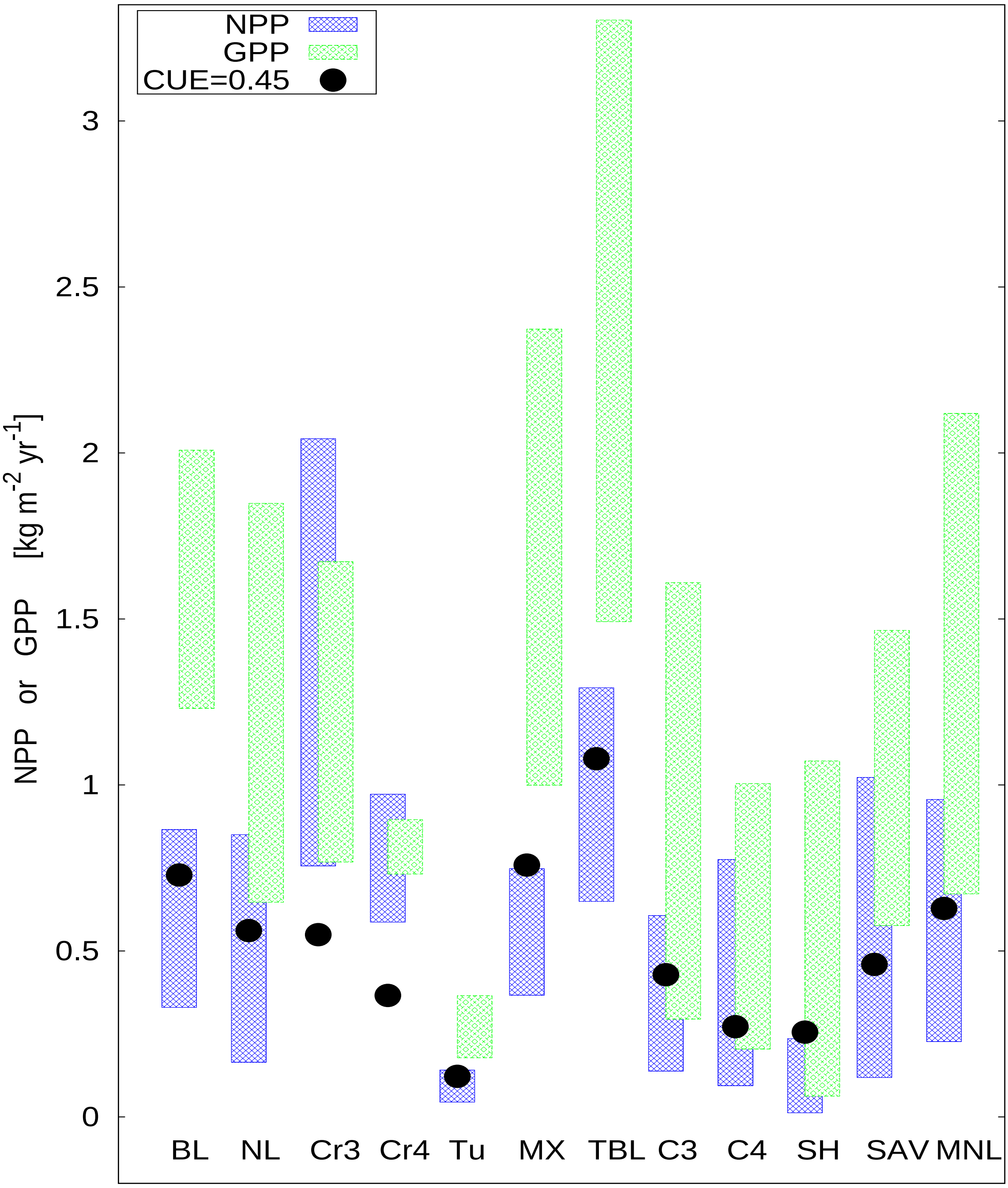

Figure 10: Estimates of Net Primary Productivity (NPP; upper panel) and Gross Primary Productivity (GPP; lower panel) for PFTs which are well represented in terms of the original sample size (abbreviated according to Tab. 2). To compare different vegetation types, primary productivity is expressed per unit area (kg m^{-2} yr^{-1}) by averaging over all global grid cells of the corresponding PFT. The sample size used in the weighted global calculation of GPP (FLUXNET2015 sites) or NPP (EMDI sites) is decreased systematically from approximately the maximum number of available sites to a minimum of 3. Sample selection is based on a bootstrap method without replacement. Markers represent the mean across the bootstrap samples. Errorbars represent the standard deviation from the mean and reveal the uncertainty in GPP and NPP owing to limited sampling. For clarity, markers have been slightly offset from one another horizontally.

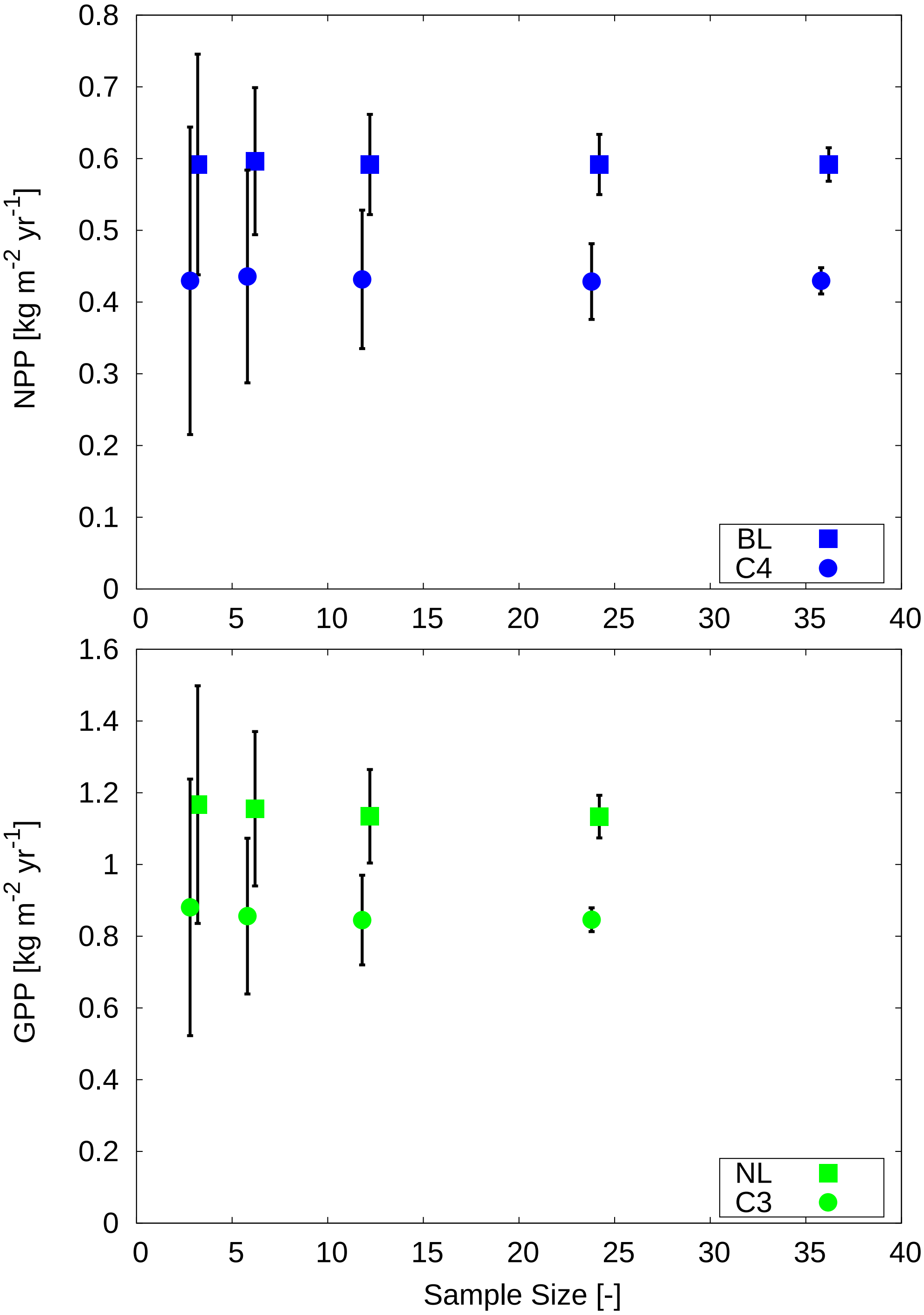

Figure 11: The GPP ratio versus NPP ratio for global vegetated 0.5° landpoints, shown separately for each PFT and labelled according to Tab. 2. The ratio equals the primary productivity simulated within the interpolated climate-canopy space, by the land-surface model JULES-SF, divided by the primary productivity simulated for the global climate-canopy space. Interpolated space depends on the distribution of carbon-monitoring sites for FLUXNET2015 and EMDI (§4.2). Similarity between the interpolated and global space should yield a ratio close to unity (dot-dash line). The dashed line (y=x) represents similar biases for NPP and GPP.